HHS Public Access

Author manuscript

*Nat Neurosci*. Author manuscript; available in PMC 2024 May 18.

Published in final edited form as:

*Nat Neurosci*. 2023 May ; 26(5): 774–787. doi:10.1038/s41593-023-01297-5.

# A hypothalamic pathway that suppresses aggression towards superior opponents

**Dongyu Wei**[1], **Takuya Osakada**[1], **Zhichao Guo**[1], **Takashi Yamaguchi**[1], **Avni Varshneya**[1], **Rongzhen Yan**[1], **Yiwen Jiang**[1], **Dayu Lin**[1,2]

[1]Neuroscience Institute, New York University Langone Medical Center, New York, NY, USA

[2]Department of Psychiatry, New York University Langone Medical Center, New York, NY, USA; Center for Neural Science, New York University, New York, NY, USA

## Abstract

Aggression is costly and requires tight regulation. Here, we identify the projection from estrogen receptor alpha expressing cells in the caudal part of the medial preoptic area (cMPOA$^{Esr1}$) to the ventrolateral part of the ventromedial hypothalamus (VMHvl) as an essential pathway for modulating aggression in male mice. cMPOA$^{Esr1}$ cells increase activity mainly during male–male interaction, which differs from the response pattern of rostral MPOA$^{Esr1}$ (rMPOA$^{Esr1}$) cells during male–female interactions. Notably, cMPOA$^{Esr1}$ cell responses to male opponents correlated with the opponents' fighting capability, which mice could estimate based on physical traits or learn through physical combats. Inactivating the cMPOA$^{Esr1}$–VMHvl pathway increased aggression, whereas activating the pathway suppressed natural inter-male aggression. Thus, cMPOA$^{Esr1}$ is a key population for encoding opponents' fighting capability — information that could be used to prevent animals from engaging in disadvantageous conflicts with superior opponents by suppressing the activity of VMHvl cells essential for attack behaviors.

## Introduction

Aggression is an innate social behavior essential for defending territory, competing for resources, and securing mating opportunities. However, aggression is a costly and consequential behavior, and individuals need to avoid disadvantageous fights to survive and reproduce. When aggression is directed toward a stronger opponent, i.e., animals with higher resource holding potential (RHP), it could lead to severe physical damage or even death[1].

Correspondence: dayu.lin@nyulangone.org.

Author Contributions Statement

D.L. conceived the project, designed experiments, analyzed data and wrote the paper. D.W. co-designed and performed most experiments, analyzed data, prepared figures and co-wrote the paper. T.O. and T.Y. performed some tracing experiments. T.O. and Y.J. performed some behavior tests and animal tracking. Z.G. performed some photometry recordings. A.V. assisted with histology analysis and animal behavior training. R.Z. performed some behavior tests to quantify the RHP of animals with different genetic background.

Competing Interests Statement

The authors declare no competing interests.

Code availability

MATALB code used in this study can be downloaded from 10.5281/zenodo.7700343.

While several nodes essential for driving aggression have been identified[2–5], the neural circuit that directs aggression away from superior social targets remains largely unknown.

The ventrolateral part of the ventromedial hypothalamus, especially cells expressing estrogen receptor alpha (VMHvl$^{Esr1}$), is an indispensable population for inter-male aggression[6–8]. Its activation can drive attack and increase aggressive motivation, whereas its inactivation suppresses natural inter-male aggression[6–10]. Retrograde tracing revealed over 20 brain regions projecting densely to the VMHvl, and the medial preoptic area (MPOA) represents the No. 1 source of input to VMHvl$^{Esr1}$ cells[11,12].

MPOA is a hypothalamic region located anterior to the VMHvl, and similar to VMHvl, it expresses abundant Esr1. MPOA$^{Esr1}$ cells have been found to be essential for sexual and parental behaviors[12–14]. However, its relevance to aggression is controversial. Early studies suggested a positive role of MPOA in aggression, as electric lesions of MPOA inhibited male aggression in rodents[15–18]. Later, several studies reported no change in aggression after MPOA manipulation. Specifically, knocking down Esr1 in MPOA or ablating MPOA$^{Esr1}$ cells did not alter male aggression, although these manipulations effectively suppressed male sexual behaviors[12,19]. Most recently, the MPOA was suggested to suppress aggression. Optogenetic activation of the projection from MPOA GABAergic Esr1 expressing cells to the VMHvl reduced inter-male aggression. However, silencing the cells had little impact on inter-male aggression[14]. Altogether, the function of MPOA in inter-male aggression remains elusive even though it is well positioned to modulate aggression anatomically.

Here, we demonstrated distinct response patterns of rostral and caudal MPOA$^{Esr1}$ cells (rMPOA$^{Esr1}$ and cMPOA$^{Esr1}$), with cMPOA$^{Esr1}$ cells responding preferentially during inter-male encounters. Interestingly, the response of cMPOA$^{Esr1}$ cells to a male opponent depends on the perceived RHP of the opponent. The RHP-dependent response of cMPOA$^{Esr1}$ cells is functionally important as activities of cMPOA$^{Esr1}$ cells could modulate inter-male aggression bi-directionally through its influence on VMHvl cells.

## Results

### Distinct responses of rMPOA$^{Esr1}$ and cMPOA$^{Esr1}$ cells

MPOA$^{Esr1}$ cells have been established as an important population for male sexual behaviors[12,14,19]. Immediate early gene mapping and *in vivo* recording suggest that MPOA$^{Esr1}$ cells are highly activated during male sexual behaviors, and activities of the cells can bi-directionally modulate male mounting[12,14]. However, the sexual behavior-induced c-Fos is not evenly distributed in the MPOA. It is concentrated in the rostral part of MPOA (rMPOA)[20]. By contrast, the caudal part of MPOA (cMPOA) expresses more c-Fos after agonistic inter-male interaction than male sexual behaviors[20]. To examine the potential heterogeneity in MPOA$^{Esr1}$ cell responses during social behaviors, we performed fiber photometry recording of MPOA$^{Esr1}$ $Ca^{2+}$ signal using 100-μm optic fibers, which collect signal from a smaller volume compared to the typically used 400-μm fibers (Fig. 1a, b). Consistent with c-Fos results, rMPOA$^{Esr1}$ cells (Bregma level 0.14 mm) showed higher responses during introduction of a female than a male intruder, whereas cMPOA$^{Esr1}$ cells (Bregma level −0.3 mm) showed similar $Ca^{2+}$ responses in the two conditions (Fig.

1b–e). Moreover, rMPOA$^{Esr1}$ cells showed significantly higher increases during female investigation than male investigation, whereas cMPOA$^{Esr1}$ cells overall responded little (Fig. 1f–h). When the male mounted the female, rMPOA$^{Esr1}$ cells increased activity acutely whereas cMPOA$^{Esr1}$ cells did not (Fig. 1i–k). Lastly, when the recording mice attacked the male intruder, cMPOA$^{Esr1}$ cells, but not rMPOA$^{Esr1}$ cells, increased activity (Fig. 1i–k). These results suggest that rMPOA$^{Esr1}$ and cMPOA$^{Esr1}$ cells are activated during different social contexts. In particular, unlike rMPOA$^{Esr1}$, cMPOA$^{Esr1}$ is minimally involved in male sexual behaviors.

## cMPOA$^{Esr1}$ cells encode male opponents' RHP

While cMPOA$^{Esr1}$ cells respond minimally during male investigation in naïve males, the cells show higher responses when a defeated animal is re-exposed to the winner of the fight. Specifically, we examined c-Fos expression in the MPOA induced by interaction with a cupped aggressor in animals that either had been previously defeated by the same aggressor or had interacted with it through a barrier for two days (Extended Data Fig. 1a). Compared to the interaction-only animals, defeated animals spent less time approaching and investigating the cupped aggressor and more time next far from the aggressor (Extended Data Fig. 1b–e). Despite the reduced interaction, the cupped aggressor induced more c-Fos in the cMPOA in the defeated animals than interaction-only animals (Extended Data Fig. 1f, g). By contrast, c-Fos expression in the rMPOA did not increase with defeat experience (Extended Data Fig. 1f, g).

This result suggests that the cMPOA$^{Esr1}$ cell response to male conspecifics is plastic: it increases once the animals recognize the male as a stronger opponent. We thus hypothesized that cMPOA$^{Esr1}$ cells may modulates aggression based on the perceived RHP of the opponent. RHP, coined by G.A. Parker, is a measure of the ability of an animal to win an all-out fight if one were to take place[1]. RHP can be assessed based on physical traits, e.g., body size and weaponry, but more reliably through physical combats[1]. It is advantageous for animals to avoid fighting with an opponent whose RHP is substantially higher than its own to minimize damage and increase chances of survival.

To further address whether cMOPA$^{Esr1}$ cells may carry RHP information of an opponent, we used fiber photometry to record the responses of cMOPA$^{Esr1}$ cells to male opponents with different RHPs. We virally expressed GCaMP6f in the cMPOA$^{Esr1}$ cells and recorded cell responses as the test mouse (Esr1$^{Cre}$ in C57BL/6 background) explored a big square arena that contained an empty cup and three cupped animals with different levels of RHP, including a non-aggressive group-housed Balb/C male, a C57BL/6 male with experiences similar to the test mouse and an aggressive single-housed SW male (Fig. 2a–2d). We estimated the RHP (ranging from 0–1 with high values indicating high RHP) of each type of stimulus mouse relative to the test mouse based on the fighting outcomes between the mice of the same kinds, i.e., single-housed SW vs. single-housed C57 and group-housed BC vs. single-housed C57 (Extended Data Fig. 2). The RHPs of the SW and BC mice relative to C57 were 0.94 and 0.27, respectively. The RHP of the stimulus C57 was assumed to be 0.5, given that they have the same genetic background and similar social experience as the test mouse (Extended Data Fig. 2). The higher RHP of the SW aggressor was also evident based

on the animal's body weight: SW aggressors weighed (mean ± STD: 42.9 ± 7.6 g, n=13) approximately 40% higher than Balb/C (mean ± STD: 29.2 ± 1.9 g, n=17) and C57BL/6 male mice (mean ± STD: 27.2 ± 2.1g, n=10).

During the test, the recording animal freely visited the cups and investigated each of the cupped males repeatedly through the metal wires (Fig. 2d). Although the total time spent around a cup and the investigation time was not significantly different among cups, the interaction time with the cupped SW male tended to be low (Fig. 2f, h). When the recording animal investigated an empty cup, there was no significant activity change in cMPOA$^{Esr1}$ cells (Fig. 2k). During the investigation of a cupped male, the $Ca^{2+}$ response of cMPOA$^{Esr1}$ cells was generally low, despite some variability in responses during SW investigation across recording animals (Fig. 2i, l–n, p).

After the 4-cup interaction test, the same non-aggressive Balb/C male and aggressive SW males were introduced as intruders into the recording animal's home cage, one at a time for 10 minutes each, on three consecutive days (Fig. 2c). The Balb/C male intruder never attacked. By contrast, the SW male attacked the test mice repeatedly. Towards the end of the first SW intruder session, the SW was a clear winner as it initiated all attacks while the test mouse spent most time staying in the corner, freezing or showing an upright submissive posture. The recording animal clearly recognized the SW aggressor the day after the last resident–intruder (R–I) test. In a subsequent 4-cup test, the recorded mice now spent less time around or investigated the cupped SW male and more time around the empty cup compared to the pre-defeat level (Fig. 2e–h). The investigation time with non-aggressive BC and C57 males was not significantly altered (Fig. 2e–h).

After the defeat experience with the SW aggressor, we found that the response of cMPOA$^{Esr1}$ cells to the same cupped SW male was significantly increased from the pre-defeat level, while responses to other male mice remained unchanged (Fig. 2i, j, l–o). Across animals, the responses of cMPOA$^{Esr1}$ cells were significantly higher towards the SW aggressor than Balb/C and C57 mice after the defeat but not before defeat (Fig. 2p). When considering all responses together, we noticed a significant negative correlation between the time around the cup and the response magnitude after defeat, that is, the higher the response of cMPOA$^{Esr1}$ cells during investigating a male, the less time the test animal spent around that male (Fig. 2r). Interestingly, this correlation appeared to exist even before defeat: in the subset of test animals that already showed slight avoidance of the SW male before defeat, the response of cMPOA$^{Esr1}$ cells during investigating of the SW male was relatively high (Fig. 2q). These results suggest that cMPOA$^{Esr1}$ cells encode information regarding the perceived RHP of an opponent, which could be either learned from fighting experience or perhaps estimated based on physical traits of an opponent, such as body size.

## cMPOA$^{Esr1}$ cells bi-directionally modulate male aggression

To understand the functional importance of the increased cMPOA$^{Esr1}$ cell responses, we chemogenetically manipulated cMPOA$^{Esr1}$ cell activity and examined changes in aggressive behaviors. Specifically, we injected AAVs expressing Cre-dependent hM4Di-mCherry, hM3Dq-mCherry, or mCherry into the cMPOA of Esr1$^{Cre}$ male mice and referred to them as cMPOA$^{hM4Di}$, cMPOA$^{hM3Dq}$, and cMPOA$^{mCherry}$ mice, respectively (Fig. 3a, b). The

virus expression was centered in the cMPOA but also spread to rMPOA (Fig. 3b). Thus, we considered the manipulation as cMPOA-biased but not cMPOA-exclusive. Three weeks after virus injection, the test animals were subjected to a resident–intruder (R–I) assay until the aggression level was stabilized or up to 7 days of testing (some animals never became aggressive) (Fig. 3c). Then, we injected saline on the first day and CNO (1 mg/kg) on the second day for all animals and examined their aggression level towards a non-aggressive male intruder. Compared to saline-injected days, CNO injection into cMPOA$^{hM4Di}$ animals significantly decreased attack latency and increased total attack duration without changing the total investigation duration or pre-intruder locomotion velocity (Fig. 3d, e). Strikingly, CNO injection into cMPOA$^{hM4Di}$ animals also induced repeated attacks towards Balb/C female intruders, whereas no test animal attacked females after saline injection (Fig. 3f, g). However, cMPOA$^{Esr1}$ inhibition only enhanced aggression in naturally aggressive animals: inhibiting the cells did not induce attack in non-aggressive animals, although it increased social-investigation time (Extended Data Fig. 3).

In contrast to the results of cMPOA$^{hM4Di}$ animals, CNO injection into cMPOA$^{hM3Dq}$ animals, i.e., cMPOA$^{Esr1}$ cell activation, nearly abolished inter-male aggression. Only 5/10 animals initiated attacks toward a male intruder, and each animal attacked only for a few seconds. By contrast, after saline injections, all test animals attacked the male intruder repeatedly and quickly (Fig. 3h, i). Across all animals, attack duration significantly decreased, whereas attack latency significantly increased (Fig. 3i1–i2). The decrease in attack duration was not due to a general loss of interest in the intruder or compromised movement, as the total investigation time and locomotion velocity did not differ between saline- and CNO-injected days (Fig. 3i3, i4). None of the cMPOA$^{hM4Di}$ males attacked females after either saline or CNO injection and spent a similar amount of time investigating the females (Fig. 3j, k). cMPOA$^{mCherry}$ animals showed no difference in investigation, aggression, or locomotion between saline- and CNO-injected days (Fig. 3l–o). These results suggest that cMPOA$^{Esr1}$ cells negatively modulate male aggression.

## cMPOA$^{Esr1}$ cells primarily inhibit VMHvl$^{Esr1}$ cells

Given that MPOA contains the largest number of retrogradely labeled cells from VMHvl$^{Esr1}$ and VMHvl$^{Esr1}$ plays an important role in male aggression[6,8,11,21], we hypothesized that cMPOA$^{Esr1}$ cells modulate aggression through their projection to VMHvl$^{Esr1}$ cells. To test this hypothesis, we first performed anterograde virus tracing from cMPOA$^{Esr1}$ cells and confirmed that VMHvl is among the regions that receive dense projection from cMPOA$^{Esr1}$ cells (Extended Data Fig. 4). We then performed monosynaptic rabies retrograde tracing from VMHvl$^{Esr1}$ cells and found that MPOA contains densely labeled cells throughout its anterior-posterior axis (Extended Data Fig. 5).

To confirm a functional connection between cMPOA$^{Esr1}$ cells and VMHvl$^{Esr1}$ cells, we performed channelrhodopsin (ChR2)-assisted circuit mapping on brain slices (Fig. 4a). We injected Cre-dependent ChR2-eYFP into the cMPOA and Cre-dependent mCherry into the VMHvl of Esr1$^{Cre}$ male mice. Three weeks later, we performed patch clamp recording of VMHvl mCherry+ cells (Fig. 4b, c). We found that 470-nm light pulses evoked strong inhibitory postsynaptic currents (oIPSCs) in every recorded cell, and 28% (12/43) of cells

also showed light-evoked excitatory postsynaptic currents (oEPSCs), consistent with the fact that MPOA$^{Esr1}$ cells are approximately 80% GABAergic and 20% glutamatergic (Fig. 4d1, d2)[12,13]. Across the recorded cells, oIPSCs were larger in amplitude than oEPSCs and with slightly but significantly shorter latencies (Fig. 4d3, d4). When we applied tetrodotoxin (TTX) and 4-Aminopyridine (4-AP), which blocks polysynaptic transmission, neither oIPSC nor oIPSC changed the amplitude significantly (Fig. 4e, f), supporting the monosynaptic nature of the connections.

Do GABAergic inputs from MPOA decrease while glutamatergic inputs increase the VMHvl output? Answering this question is complicated by the fact that VMHvl and its surrounding regions contain not only glutamatergic but also GABAergic cells. The majority of VMHvl$^{Esr1}$ cells are glutamatergic, but some are GABAergic[22]. Additionally, the tuberal nucleus (TU), an area next to the VMHvl, contains mainly GABAergic cells (Fig. 4g)[23]. Anterograde tracing from MPOA$^{Esr1}$ cells revealed dense projections not only in the VMHvl but also in TU (Extended data Fig. 4d). Our Chrimson-assisted circuit mapping showed that the GABAergic cells in and surrounding the VMHvl provide strong inhibitory inputs to 100% putative VMHvl glutamatergic cells (Fig. 4h–j). Thus, depending on the relative input strength of MPOA cells to GABAergic and glutamatergic cells in the VMHvl and TU, MPOA input could have opposite effects on the net output of VMHvl glutamatergic cells.

To further understand the impact of GABAergic and glutamatergic cMPOA-VMHvl projections, we injected Cre-dependent Chrimson-tdTomato into the cMPOA of Vgat$^{Cre}$ × Ai6 and Vglut2$^{Cre}$ × Ai6 mice (Fig. 4k, l, n, and o). Three weeks later, we performed patch clamp recording of putative GABAergic (zsGreen+ in Vgat$^{Cre}$ × Ai6 and zsGreen− in Vglut2$^{Cre}$ × Ai6) and glutamatergic cells (zsGreen− in Vgat$^{Cre}$ × Ai6 and zsGreen+ in Vglut2$^{Cre}$ × Ai6) in VMHvl and TU on the same slice while delivering brief 605-nm light pulses to activate MPOA GABAergic or glutamatergic terminals (Fig. 4m1, p1). Stimulating the GABAergic input from the cMPOA evoked IPSCs in all recorded cells in the VMHvl and TU (Fig. 4m2). However, the oIPSC amplitude was significantly higher in putative glutamatergic cells than GABAergic cells, while the latency of oIPSCs was similarly short, suggesting MPOA GABAergic inputs target VMHvl glutamatergic cells preferentially (Fig. 4m). An opposite pattern was observed for the MPOA glutamatergic projection (Fig. 4p). Only 4/15 VMHvl glutamatergic cells (zsGreen+) showed oEPSCs and the amplitude was generally low, whereas the majority (14/18) of putative GABAergic cells showed oEPSCs with higher amplitude (Fig. 4p2, p3). The latencies of the oEPSCs recorded from glutamatergic and GABAergic cells were similarly short (Fig. 4p4). Thus, cMPOA glutamatergic cells preferentially target GABAergic VMHvl/TU cells. These results suggest that both GABAergic and glutamatergic inputs from cMPOA primarily inhibit VMHvl glutamatergic cells, either directly or indirectly via the local inhibitory circuit (Fig. 4q).

## cMPOA$^{Esr1}$ cells modulate VMHvl activity bidirectionally

We next asked whether cMPOA$^{Esr1}$ cell activity can influence the activity of VMHvl$^{Esr1}$ cells *in vivo* by injecting AAVs expressing Cre-dependent hM4Di-mCherry, hM3Dq-mCherry, or mCherry into cMPOA and GCaMP6f into ipsilateral VMHvl of Esr1$^{Cre}$ male mice (Fig. 5a, b). An optic fiber was implanted above the VMHvl to record the population

$Ca^{2+}$ activity of $VMHvl^{Esr1}$ cells (Fig. 5a, b). Three weeks later, we trained the animals on R-I tests until they show stable aggression, and then injected saline and CNO on separate days while recording GCaMP6f signals continuously using fiber photometry (Fig. 5c, d). We focused on the spontaneous $VMHvl^{Esr1}$ cell activity in solitary animals to separate changes in neural activity from changes in social behaviors induced by $cMPOA^{Esr1}$ manipulation.

In $cMPOA^{hM4Di}$ animals, CNO injection significantly increased the frequency of $VMHvl^{Esr1}$ $Ca^{2+}$ transients and the peak magnitude of the transients compared to saline injection, (Fig. 5e, h, i). The fact that suppressing $cMPOA^{Esr1}$ cells increases the spontaneous activity of $VMHvl^{Esr1}$ cells suggests that $MPOA^{Esr1}$ cells exert tonic inhibition onto $VMHvl^{Esr1}$ cells. Conversely, CNO injection into $cMPOA^{hM3Dq}$ animals significantly reduced the frequency of $VMHvl^{Esr1}$ cell $Ca^{2+}$ transients compared to saline injection, although the magnitude of the transients remained unchanged (Fig. 5f, h, i). Lastly, $cMPOA^{mCherry}$ animals showed no significant difference in $VMHvl^{Esr1}$ $Ca^{2+}$ transients after CNO and saline injections (Fig. 5g, h, i).

## Activating $cMPOA^{Esr1}$-VMHvl pathway suppresses aggression

To address whether the $cMPOA^{Esr1}$-VMHvl projection is sufficient to modulate aggression, we injected viruses expressing Cre-dependent ChR2-eYFP into the cMPOA bilaterally and implanted bilateral 200-μm optic fibers above the VMHvl of $Esr1^{Cre}$ male mice on a C57 background (Fig. 6a, b). Histology analysis showed that the ChR2 expression centered in the cMPOA (Fig. 6b). Three weeks later, the animals were exposed to male intruders daily for 3–7 days until they showed aggressive behaviors consistently. On the testing day, we introduced a male intruder and delivered 20-s blue light pulses (20ms, 20Hz, 1–2mW) or sham light (0 mW) whenever the test mouse initiated an attack toward the intruder (Fig. 6c). Upon light delivery, the test mouse immediately terminated ongoing attack (mean latency to stop the attack: 0.1 s), whereas it took approximately 1.3 s for the attack to stop naturally (Fig. 6d–h). During the light-on period, the probability of attack re-initiation also significantly decreased in comparison to that during sham trials (Fig. 6i). Altogether, the total attack duration was significantly lower during light trials than during sham trials (Fig. 6j). Although the animals stopped attacking upon light delivery, they continued to interact with the intruder. Consequently, the total investigation duration increased in light trials compared to sham trials (Fig. 6k). Increased investigation duration was also observed in our previous studies when ongoing social behavior was terminated artificially and abruptly[24,25], possibly reflecting the natural tendency of animals to be socially engaged when they are in close proximity. Control mCherry animals showed no difference in investigatory or aggressive behaviors during sham vs. light trials (Fig. 6d–k). Interestingly, we noticed that ChR2 animals tended to spend more time attacking the intruder in sham trials in comparison to control animals (Fig. 6j), and the total attack duration during the entire test session was similar between the two groups, suggesting compensatory attacks in ChR2 animals after their attack effort was halted abruptly in light trials (Fig. 6l).

To understand whether or not the suppression effect of $MPOA^{Esr1}$-VMHvl activation on aggression is experience-dependent, we repeated the experiment using naïve $Esr1^{Cre}$ mice on an SW background (Extended Data Fig. 6). Most SW mice are naturally aggressive;

thus, no training or screening was performed to pre-determine their aggression level. We found that MPOA$^{Esr1}$-VMHvl activation similarly suppressed attack in naïve aggressive SW males, suggesting that the wiring of this pathway does not require adult fighting experience (Extended Data Fig. 6).

## Inhibiting cMPOA$^{Esr1}$-VMHvl pathway enhances aggression

We next asked whether optogenetic inhibition of the MPOA$^{Esr1}$–VMHvl projection is sufficient to promote aggressive behaviors by expressing stGtACR2-FusionRed (Control: mCherry) in the cMPOA bilaterally and implanted optic fibers above the VMHvl in Esr1$^{Cre}$ male mice on a C57 background (Fig. 7a, b). Histology analysis showed that stGtACR2-FusionRed expression centered in the cMPOA with some spread to rMPOA (Fig. 7b). Three weeks after surgery and on the testing day, we interleaved light (20 ms, 20 Hz, 0.5–2 mW, 20 s) and sham trials (0 mW, 20 s) starting from 1~3 minutes after introducing a Balb/c non-aggressive male intruder (Fig. 7c). In stGtACR2 animals, the probability of attack initiation during light trials was significantly higher than that during sham trials (Fig. 7d–h). For sham trials with attack, the latency to attack was significantly longer than that during light trials (Fig. 7i). Overall, stGtACR2 animals spent significantly more time attacking during light than sham trials while the investigation duration remained the same (Fig. 7j, k). The total duration of attack in the 10 minutes test session was significantly higher in stGtACR2 animals than mCherry animals (Fig. 7l). Strikingly, inhibiting MPOA$^{Esr1}$ to VMHvl projection also promoted attack towards female intruders (Fig. 7m–u). After the female introduction, no male attacked the female spontaneously before light delivery. During light stimulation, 7/7 stGtACR2 males initiated attacks in 63% of trials with an average latency of approximately 4 s, whereas none of the mCherry mice attacked the female (Fig. 7q, r). After repeated light stimulation, the males occasionally attacked the female during sham trials, although the duration was significantly shorter than that of light stimulation trials (Fig. 7q, r, s). The investigation duration between light and sham trials were similar for both stGtACR2 and mCherry animals (Fig. 7t). Overall, stGtACR2 animals spent a similar amount of time attacking male and female intruder during the test session. By contrast, mCherry animals attacked male intruders exclusively (Fig. 7l, u). Consistent with the MPOA$^{Esr1}$ inhibition results, MPOA$^{Esr1}$–VMHvl inhibition only promoted attack in aggressive animals. In non-aggressive animals, the manipulation did not induce attacks towards either male or female intruders (Extended Data Fig. 7).

To understand whether the cMPOA$^{Esr1}$–VMHvl pathway carries valence information, we performed a real-time place preference test (RTPP) and found that both ChR2 and stGtACR2 animals avoided the light-paired chamber while mCherry control animals did not, suggesting that either too much or too little activity of this pathway is aversive to the animal (Extended Data Fig. 8). Given that cMPOA$^{Esr1}$–VMHvl activation and inactivation caused an opposite change in aggression but a similar change in valence, these two behavior phenotypes appear to be orthogonal to each other.

## cMPOA$^{Esr1}$-VMHvl inhibition evokes attack to superior males

Lastly, we asked whether inhibiting cMPOA$^{Esr1}$ cells could increase aggression towards superior opponents. This is an important question, given that superior opponents are the

animals that naturally activate cMPOA$^{Esr1}$ cells. First, we confirmed that even a single 10-min defeat experience is sufficient to suppress aggression towards the winner (Extended Data Fig. 9). In a group of 7 C57BL/6 mice that attacked non-aggressive male Balb/C intruder readily, none initiated attack towards the SW aggressor 24 hours after being defeated by the SW while they remained aggressive towards Balb/C intruders (Extended Data Fig. 9).

Next, we examined the behavior of the defeated animal towards the winner when the cMPOA$^{Esr1}$ to VMHvl pathway was optogenetically inhibited (Fig. 8a–c). As expected, without light stimulation, both mCherry and stGtACR2 mice rarely initiated attacks toward the SW aggressor after defeat (Fig. 8d, f). However, with light stimulation (20 ms, 20 Hz, 0.5–2 mW, 20 s), stGtACR2 mice, but not mCherry mice, initiated attacks towards the SW aggressor in 58% of trials, with an average attack latency of 7.6 s (Fig. 8e, g–i). The average duration of offensive attack initiated by the stGtACR2 mice was significantly higher during light trials than during sham trials (Fig. 8j).

Interestingly, although inhibiting cMPOA$^{Esr1}$ to VMHvl pathway increased attack towards all intruders, the pattern of attack differed based on the intruder type. Light stimulation mainly increased lunge and tumble when stGtACR2 mice encountered BC male and C57 female intruders (Fig. 8n–o), whereas the same manipulation mainly increased bites towards the SW intruder (Fig. 8p). This suggests that MPOA$^{Esr1}$–VMHvl pathway does not control a specific component of attack. Instead, it modulates the attack tendency, and the animals remain flexible in choosing the attack strategy during the stimulation.

Furthermore, the stGtACR2 mice spent more time attacking the SW defensively during light stimulation when they were being attacked, whereas control animals rarely fought back (Fig. 8k). But likely due to light-induced behavior changes of stGtACR2 mice, SW aggressors spent more time attacking stGtACR2 mice, but not mCherry mice, during the light-on period; as a result of the increased aggression of SW mice and difference in physical strength, stGtACR2 mice were ultimately defeated for a longer period during light stimulation (Fig. 8l, m). These results provide evidence for a role of cMPOA$^{Esr1}$ cells in suppressing aggression towards animals with superior fighting capability based on previous fighting outcomes, possibly in an effort to minimize provocation and reduce the physical damage the superior opponent could inflict.

## Discussion

In our study, we revealed a neural pathway that helps male mice to pick the right fight. We found that cMPOA$^{Esr1}$ cells encode the perceived RHP of an opponent and can use this information to direct aggression away from a superior opponent through its inhibition onto VMHvl, a key region for driving aggression. When this pathway was inactivated, males initiated more attacks toward a superior opponent and only ended up getting defeated more. Importantly, cMPOA$^{Esr1}$ cells can update the opponent's RHP information based on fighting outcomes. Thus, cMPOA$^{Esr1}$–VMHvl projection could be a key mechanism that enables the animals to individualize their behaviors towards each member in a complex social group based on the history of agonistic interactions.

## Heterogeneity of MPOA subregions

MPOA is a large area spanning approximately 0.5 mm along the anterior-posterior axis. Esr1 expression in the MPOA is mainly concentrated in the medial preoptic nucleus (MPN), an oval-shaped cell dense area situated in the center of MPOA, and striohypothalamic nucleus (StHy), a cluster dorsal to the MPN[26,27]. Detailed molecular profiling of single MPOA cells revealed dozens of molecularly distinct clusters within preoptic Esr1 cells[22,27]. Consistent with our finding that rMPOA$^{Esr1}$ and cMPOA$^{Esr1}$ cells show differential *in vivo* responses, some molecularly defined Esr1 clusters are concentrated in the rMPOA while others show caudal bias, although no cluster shows exclusive expression in one subregion[27]. Furthermore, a higher percentage of rMPOA$^{Esr1}$ cells are glutamatergic than cMPOA$^{Esr1}$ cells[14,27,28]. These results collectively support regional differences within the MPOA, although this difference is likely a gradual shift instead of a sudden switch.

In previous tracing studies focusing on MPOA, rMPOA-centered and cMPOA-centered injections were achieved, but connectivity difference was not reported and thus may imply a lack of such[29,30]. Here, our monosynaptic rabies tracing from VMHvl$^{Esr1}$ cells revealed abundant retrogradely labeled cells in both rMPOA and cMPOA, suggesting that VMHvl$^{Esr1}$ cells receive strong inputs from the entire MPOA. Indeed, rMPOA$^{Esr1}$ and cMPOA$^{Esr1}$ cells likely both play a role in suppressing aggression through their projections to the VMHvl, although these two pathways could be naturally engaged under different social contexts, with the former being activated mainly during male-female interaction and the latter during male-male interaction.

## MPOA-VMHvl pathway suppresses aggression

Despite early lesion studies that suggest a role of MPOA in promoting aggression[15–18], our results indicate that MPOA$^{Esr1}$ cells suppress aggression. Chemogenetic activation of the MPOA$^{Esr1}$ cells and optogenetic activation of MPOA$^{Esr1}$–VMHvl projection nearly abolished inter-male aggression. It is worth noting that during MPOA$^{Esr1}$–VMHvl terminal stimulation, MPOA$^{Esr1}$ fibers coursing through the VMHvl to the PMv could also be activated to suppress PMv. As PMv is also important in inter-male aggression, its suppression could contribute to the decreased attack[31–33]. Under natural conditions, it is likely that MPOA$^{Esr1}$ cells modulate aggression through its projection to both VMHvl and PMv, which are strongly reciprocally interconnected[11,34]. Additionally, MPOA$^{Esr1}$–VMHvl terminal stimulation may recruit MPOA$^{Esr1}$ cell bodies to some extent due to backpropagation of action potentials and affect other downstream areas, e.g., BNSTpr, a region that was recently identified to promote male aggression possibly through its dense projections to the VMHvl and PMv[32,35–37]. Indeed, MPOA, VMHvl, PMv, and BNSTpr all belong to the heavily interconnected social brain network[2,38]. Alternating activity in one pathway likely results in activity changes in the entire network, collectively leading to behavioral changes.

In contrast to the behavior change of cMPOA$^{Esr1}$ activation, inactivating cMPOA$^{Esr1}$ cells or cMPOA$^{Esr1}$–VMHvl pathway increased aggression. It is important to note that although inactivating cMPOA$^{Esr1}$–VMHvl affects aggression towards various social targets, we consider the primary endogenous role of the cMPOA$^{Esr1}$–VMHvl pathway as to suppress

aggression towards superior opponents. This conclusion is based on the fact that male cMPOA$^{Esr1}$ cells are minimally activated by females and weak males naturally but are strongly excited by superior males. During artificial manipulation, however, the activity of MPOA$^{Esr1}$ cells, and consequently the activity of VMHvl cells, was altered regardless of the social target, causing target-unspecific changes in aggression. Indeed, artificial activation of VMHvl cells could evoke attack towards unnatural targets, including females[6,7,10]. Furthermore, our functional manipulation also engaged some rMPOA cells. Thus, the increased aggression towards females could also reflect reduced inhibition from rMPOA to VMHvl, which may naturally suppress male aggression towards females.

While we observed an apparent increase in aggression after inactivating MPOA$^{Esr1}$ cells, a recent study reported no reliable increase in aggression after chemogenetic inactivation of MPOA$^{Esr1}$ cells, although that study also found a decrease in inter-male aggression after optogenetic activation of MPOA$^{Esr1}$–VMHvl pathway[14]. This discrepancy could be due to differences in test animals' aggression levels and/or the manipulation site. Here, we found that the inactivating MPOA$^{Esr1}$ cells only increased attack in aggressive but not non-aggressive males, suggesting a positive correlation between the aggression-promoting effect of MPOA$^{Esr1}$ inactivation and the animal's natural aggression level. At the circuit level, MPOA projects to and receives dense inputs from the VMHvl[29]. Thus, the baseline suppression from MPOA to VMHvl is likely proportional to the spontaneous activity of VMHvl cells, which increases with the animal's aggression level[39]. Thus, MPOA$^{Esr1}$ cells likely inhibit the VMHvl cells more strongly in more aggressive animals due to more robust excitatory inputs from the VMHvl. Therefore, inactivating MPOA$^{Esr1}$ cells in aggressive animals could have a stronger disinhibitory effect on VMHvl cell activity. Additionally, the higher efficiency of our MPOA$^{Esr1}$ inactivation in promoting aggression may be due to the difference in targeting sites. Our manipulation centered on the cMPOA, while previous studies targeted mainly rMPOA[14]. Nevertheless, consistent with our current findings, it was noted in the previous study that "In rare cases, we have observed that silencing MPOA releases aggression towards females"[14].

### cMPOA$^{Esr1}$ cells encode the perceived RHP of opponents

Before defeat, male cMPOA$^{Esr1}$ cells generally showed low responses to other male conspecifics, although cMPOA$^{Esr1}$ cell activity during SW investigation was relatively high in the subset of animals that mildly avoided the SW aggressor. The avoidance behavior indicated that the test mouse recognized the SW as a potential threat, i.e., an opponent with a high RHP. As the test animal had never encountered SW before the test, such recognition is presumably based on the physical traits of the SW. Indeed, dominant and subordinate males differ in their body odor and body size, and body size strongly predicts fighting capability and the likelihood of winning[40,41]. cMPOA$^{Esr1}$ cells may be wired to be preferentially sensitive to physical features indicative of high RHP. However, since only some but not all naïve animals showed increased cMPOA$^{Esr1}$ cell activity to SW aggressor and behavioral avoidance, such response may be acquired through early-life experience.

After the defeat, cMPOA$^{Esr1}$ cells significantly increased responses to the winner in future encounters. What might be the neural mechanisms supporting this change in response?

In essence, defeat is an associative learning process during which specific aggressor cues become tightly linked to the painful experience of defeat[42]. At the neural level, this association process likely involves synaptic plasticity that enables the sensory cues of an aggressor, possibly olfactory, to gain access to cMPOA$^{Esr1}$ cells. Anatomically, MPOA receives abundant pheromone and volatile-related information via direct projections from the medial amygdala and bed nucleus of stria terminalis[29]. The olfactory inputs that co-occur with cMPOA$^{Esr1}$ cell activation during defeat may lead to potentiation of the synapses carrying the olfactory information of the aggressor. Consistent with this model, MPOA cells show a high c-Fos expression level after defeat[43–45]. Such Hebbian synaptic plasticity has been recently described in VMHvl$^{Esr1}$ cells: repeated pairing of excitatory inputs from the amygdala with VMHvl$^{Esr1}$ cell activation induced long-term potentiation of the amygdala inputs[39]. Future studies may reveal whether the same mechanism occurs at the MPOA to increase the cell responses to aggressor cues after defeat and consequently enable the MPOA to suppress aggression towards opponents with high RHP.

While aggression is an important social behavior to compete for resources, picking the wrong fight can have severe consequences and even cost the life of the initiator. Indeed, aggression and its underlying neural circuit are tightly modulated by the environment, opponent, and social experience[10,39,46,47]. Our study adds to these previous works by revealing an important hypothalamic pathway that directs aggression away from stronger opponents to avoid disadvantageous conflict. It provides a glimpse of the innate yet flexible subcortical social circuit that could support consequential fighting decisions in a complex social group.

## Methods

### Animals

All procedures were approved by the NYULMC Institutional Animal Care and Use Committee (IACUC) in compliance with the National Institutes of Health (NIH) Guidelines for the Care and Use of Laboratory Animals. Adult male mice (8–16 weeks) were used as test subjects for all studies. Mice were housed under a 12 h light-dark cycle (dark cycle, 10 a.m. to 10 p.m.), with food and water available ad libitum. Room temperature was maintained between 20 – 22 °C and humidity between 30–70%, with a daily average approximately 45%. Esr1$^{Cre}$, Vgat$^{Cre}$, and Vglut2$^{Cre}$ knock-in mice with C57BL/6 background[6,48] were purchased from Jackson Laboratory (Stock No. 017911, 016962, and 016963). Esr1$^{Cre}$ mice with Swiss Webster background (backcrossed for over 5 generations) were also used. Ai6[49] mice with C57BL/6 background were from the Jackson Laboratory (Stock No. 0007906) and crossed with Vgat$^{Cre}$ and Vglut2$^{Cre}$ mice. Stimulus animals were BALB/c male and female mice (>8 weeks), C57BL/6N male and female mice (>8 weeks) purchased from Charles River or bred in-house, and Swiss Webster male mice (>12 weeks) purchased from Taconic. Animals were assigned to various groups randomly. Stimulus BALB/c and C57BL/6N mice were group-housed. SW mice were experienced aggressors and single-housed. After surgery, all test animals were single-housed. All experiments were performed during the dark cycle of the animals.

10/33 GCaMP6, 1/9 stGtACR2, and 1/10 hM4Di animals were excluded due to incorrect fiber placement or poor virus expression.

## Viruses

AAV8-hSyn-DIO-hM4Di-mCherry ($1 \times 10^{13}$ vg/ml), AAV2-hSyn-DIO-hM3Dq-mCherry ($4 \times 10^{12}$ vg/ml), AAV2-hSyn-DIO-mCherry ($4 \times 10^{12}$ vg/ml), AAV1-hSyn1-SIO-stGtACR2-FusionRed ($2 \times 10^{13}$ vg/ml), and AAV1-CAG-Flex-GCaMP6f-WPRE-SV40 ($7 \times 10^{12}$ vg/ml) were purchased from Addgene. AAV2-hSyn-Flex-ChrimsonR-tdTomato ($6 \times 10^{12}$ vg/ml) and AAV2-EF1a-DIO-hChR2(H134R)-EYFP ($4 \times 10^{12}$ vg/ml or $6 \times 10^{12}$ vg/ml) were purchased from University of North Carolina vector core facility. AAV2-CAG-Flex-GCaMP6f-WPRE-SV40 ($2.21 \times 10^{13}$ vg/ml) was purchased from the University of Pennsylvania vector core facility. AAV8-hEF1α-DIO-Synaptophysin-mCherry ($2.5 \times 10^{13}$ vg/ml) was purchased from Massachusetts General Hospital Gene Delivery Core. AAV8-CAG-FLEX-TVA-mCherry ($2.04 \times 10^{13}$ vg/ml and diluted 2–10 times before injection) and AAV8-CAG-FLEX-oG ($8.9 \times 10^{13}$ vg/ml and diluted 20 times before injection) were purchased from Salk Institute. EnvA-G-deleted Rabies-eGFP ($1.07 \times 10^{8}$, vg/ml) (RV-EnvA-ΔG-eGFP) was purchased from Salk Institute. All viruses were aliquoted and stored at −80 °C until use.

## Stereotaxic surgery

Mice (8–12) weeks old were anesthetized with 1–1.5% isoflurane and placed in a stereotaxic apparatus (Kopf Instruments Model 1900). Viruses were delivered into the targeted brain regions through glass capillaries using a nanoinjector (World Precision Instruments, Nanoliter 2000) with a speed of 20 nL/min. Histology was obtained for all animals, and only those with correct virus expression and optic fiber placement were included in the final analysis.

For anterograde tracing experiments, 100 nL of AAV8-hEF1α-DIO-Synaptophysin-mCherry was unilaterally injected into the MPOA (Bregma: AP: −0.22 mm, ML: 0.335 mm, DV: 5 mm).

For monosynaptic rabies tracing, 130–140 nL of 1:1 to 1:5 mixed AAV8-CAG-FLEX-TVA-mCherry and AAV8-CAG-FLEX-oG was injected in the VMHvl (AP, −1.8 mm; ML, ±0.75 mm; DV: 5.78 mm). After 3–4 weeks, 270–300 nL of RV-EnvA-ΔG-eGFP was injected using the same coordinates, and histology was acquired 5–7 days later.

For slice recording experiments with $Esr1^{Cre}$ male adult mice, 100 nL of AAV2-EF1a-DIO-hChR2(H134R)-EYFP was bilaterally injected into the MPOA (AP: −0.22 mm, ML: 0.335 mm, DV: 5 mm), and 70 nL of AAV2-hSyn-DIO-mCherry was bilaterally injected into the VMHvl (AP: −1.58 mm, ML: 0.775 mm, DV: 5.65 mm). For slice recording experiments with $Vgat^{Cre}$ × Ai6 and $Vglut2^{Cre}$ × Ai6 male adult mice, 100 nL of AAV2-hSyn-Flex-ChrimsonR-tdTomato was injected into either MPOA (AP: −0.22 mm, ML: 0.335 mm, DV: 5 mm) or TU (AP: −1.58 mm, ML: 0.8 mm, DV: 5.65 mm). The brains were used for slice recording three weeks after surgery.

For chemogenetic manipulation experiments, 300 – 350 nL AAV2-hSyn-DIO-hM3Dq-mCherry or AAV8-hSyn-DIO-hM4Di-mCherry was bilaterally injected into the MPOA (AP: −0.22 mm, ML: 0.335 mm, DV: 5 mm) of $Esr1^{Cre}$ male mice to activate or silence the $MPOA^{Esr1}$ cells. Control mice were injected with 300 nL AAV2-hSyn-DIO-mCherry into the MPOA.

For optogenetic stimulation experiments, 300 nL of AAV2-EF1a-DIO-hChR2(H134R)-EYFP or AAV1-hSyn-SIO-stGtACR2-FusionRed was bilaterally injected into MPOA (AP: −0.22 mm, ML: 0.335 mm, DV: 5 mm) of $Esr1^{Cre}$ C57 male mice. In a separate batch of animals, 300 nL of AAV2-EF1a-DIO-hChR2(H134R)-EYFP was bilaterally injected into MPOA (AP: −0.27 mm, ML: 0.35 mm, DV: 5.25 mm) of $Esr1^{Cre}$ SW male mice. Control mice were injected with 300 nL AAV2-hSyn-DIO-mCherry into MPOA bilaterally. Optic fiber assemblies (Thorlabs, FT200EMT, CFLC230) were implanted 500 μm above the injection sites bilaterally and secured with dental cement (C&B Metabond, S380).

For fiber photometry recording of the $VMHvl^{Esr1+}$ population, 75 nL of AAV2-CAG-Flex-GCaMP6f-WPRE-SV40 was injected into the VMHvl (AP: −1.58 mm, ML: 0.775 mm, DV: 5.65 mm) of $Esr1^{Cre}$ male mice. For fiber photometry recording of the rostral and caudal $MPOA^{Esr1}$cells, 85 nL of AAV1-CAG-Flex-GCaMP6f-WPRE-SV40 was injected into the rMPOA (AP: 0.1 mm, ML: 0.335 mm, DV: 5 mm) and cMPOA (−0.22 mm, ML: 0.335 mm, DV: 5 mm), respectively, of $Esr1^{Cre}$ male mice. A 400-μm or 100-μm optical-fiber assembly (Thorlabs, FR400URT, CF440, and US Conec, 12599) was implanted 250 μm above the injection site and secured using dental cement (C&B Metabond, S380). All recordings started 3~4 weeks after the virus injection.

### Chemogenetic activation and inactivation

Before surgery, $Esr1^{Cre}$ male mice on a C57BL/6 background were screened with a resident-intruder (R-I) test. During the R-I test, a group-housed non-aggressive adult BALB/c male mouse was introduced into the home cage of the test mouse (resident) for 10 minutes. Test mice that showed more than 10 attacks were considered aggressive and randomly assigned into experimental and control groups and injected with corresponding viruses. All mice were singe-housed after the virus injection. Three weeks after surgery, all mice were further trained using resident-intruder tests for 3 to 7 days. During each training session, a group-housed non-aggressive adult BALB/c male mouse was introduced into the home cage of the surgery mouse for 10 minutes to allow the surgery mouse to receive attacking experience. Once the mice showed a stable high level of aggression (the latency to first attack <2 minutes for 3 consecutive days), they were intraperitoneally injected with saline, and 24 hours later, CNO (1 mg/kg, Millipore Sigma C0832). 40 minutes after saline or CNO injection, a group-housed non-aggressive BALB/c male adult mouse was introduced in the home cage of the test mouse for 10 minutes. 2~5 minutes after the male intruder was removed, a randomly selected group-housed BALB/c female adult mouse was introduced into the test's mouse home cage for 10 minutes. A subset of mice failed to show aggression after surgery with repeated R-I tests. These mice constituted the non-aggressive group and underwent the same behavior test as the aggressive mice.

## Optogenetic activation and inactivation

Test Esr1$^{Cre}$ mice on a C57BL/6 background were first screened using an R-I test, and aggressive animals were then used for surgery. Three to four weeks after surgery, all mice were further trained in a resident-intruder test for 3 to 7 days to ensure stable aggression. A separate group of Esr1$^{Cre}$ mice on an SW background was used for this experiment without pre-surgery aggression screening or post-surgery aggression training. On the test days, we connected 200-μm multimode optical fibers (Thorlabs, FT200EMT) with the implanted bilateral fiber assembly (Thorlabs, CFLC230–10) through matching sleeves (Thorlabs, ADAL1) to deliver blue light (473 nm, Shanghai Dream Lasers). During the test, a randomly selected group-housed BALB/c male adult mouse was introduced into the home cage of the test mouse. Light and sham trials (20 ms, 20 Hz, 0.5–2 mW for light trials and 0 mW for sham trials, 20 s) were interleaved and controlled by a custom circuit (OpenEx, TDT). For MPOA$^{Esr1}$–VMHvl terminal activation, all trials started when the test animal initiated an attack toward the BALB/c intruder. Each test consisted of at least 8 pairs of sham and light trials and lasted maximally one hour. For MPOA$^{Esr1}$–VMHvl terminal inhibition, all trials started when the test animal approached the BALB/c intruder. Each test consisted of at least 8 pairs of sham and light trials and lasted maximally 30 minutes. For the optogenetic inhibition experiment, 2~5 minutes after the male intruder was removed, a randomly selected BALB/c female adult mouse was introduced into the home cage of the test mouse. Similarly, light or sham light was delivered whenever the test mouse approached the female. At least 8 pairs of sham and light trials were collected for each test animal.

To determine the effect of MPOA$^{Esr1}$-VMHvl terminal inhibition on aggression towards aggressors, we first introduced a single-housed sexually experienced SW male into the home cage of the stGtACR2 (or mCherry) test mouse for 10–15 minutes. The aggressor repeatedly attacked and successfully defeated the test mouse in all cases. The day after defeat, the same SW aggressor was introduced into the home cage of the test mouse. Light (20 ms, 20 Hz, 0.5–2 mW, 20 s) and sham light (0 mW, 20 s) was delivered to the VMHvl in an interleaved fashion whenever the test animal or the aggressor approached the other animal. At least 8 pairs of sham and light trials were acquired for each animal, and the test lasted maximally 20 minutes.

A separate group of non-aggressive Esr1$^{Cre}$ C57BL/6 male adult mice was also tested for the effect of MPOA$^{Esr1}$-VMHvl terminal inhibition on Balb/C male and female interaction in the same way as the aggressive group.

## Behavioral tests and analysis

In the R-I test, an intruder male or female mouse was introduced into the test mouse's home cage for 10 minutes. The resident mouse was always single-housed. The social interaction test was performed in a clean cage. During the test, the SW aggressor was placed under a metal wire cup (radius of the cup bottom: 7.5 cm; height: 10.5 cm) at one end of the cage, and the test animal was allowed to freely explore the cage for 10 minutes or 20 minutes on the day for c-Fos induction. The test was performed inside a semi-dark behavior box (Med Associates, Inc., ENV-018MD-W). The four-cup social interaction test was performed in a quiet semi-dark room. The test area (L × W × H: 45 cm × 45 cm × 38 cm) contained four

metal wire cups, one in each corner. On two consecutive days before the test, the test animal was allowed to freely explore the arena for 20 minutes/day, and all cups were empty. On the test day, one cup was left empty, and each of the other three cups contained a stimulus mouse. The test mouse was allowed to freely explore the arena for 20 minutes. The cupped stimulus animals include (1) an SW male that was sexually experienced, single-housed, and had been shown to defeat C57 and BC male intruders in R-I tests consistently; (2) a C57 male that was single-housed, sexually naïve, and with no or one-time winning experience; (3) a BC male that was group-housed, sexually naïve, and with no winning experience.

The RHPs of single-housed SW males and group-housed BC males were estimated based on their winning probability when encountering single-housed C57 males as either residents or intruders. The RHP of each animal (e.g. C57) in a pair (e.g. C57 vs. SW) was calculated as (#win × 1 + #tie × 0.5 + #NF × 0.5 + #lose × 0)/ (#win + #tie + #NF + #lose). All animals used in the analysis were non-redundant.

Animal behaviors in all experiments were video recorded from both the side and top of the cage using two synchronized cameras (Basler, acA640–100gm) and a commercial video acquisition software (StreamPix 8, Norpix) at a frame rate of 25 frames/s. Manual behavioral annotation and tracking were performed on a frame-by-frame basis using custom software written in MATLAB (https://pdollar.github.io/toolbox/) [7]. Most videos were annotated by an experimenter who was not blind to the animal's group assignment. A subset of videos was also annotated blindly and showed high consistency (>90%) with annotations not done blindly. During annotation, the neural responses were unknown to the experimenter. "Offensive attack" was defined as a suite of actions initiated by the resident toward the male intruder, which included lunges, bites, tumble, and chase. Lunge was defined as a sudden forward thrust towards the intruder; bite was defined as seizing the intruder, typically the back skin, with teeth; tumble was defined as wrestling and rolling; chase was defined as fast locomotion when following the intruder; "Defensive attack" was defined when the SW aggressor attacked the test mouse, and the test mouse attacked back. When the SW aggressor attacked the test mouse, and the latter showed no attempt to attack back, the behavior of the test mouse was defined as "defeat". "Investigation" was defined as nose contact with any part of the intruder's body in an R-I test or any part of the cup in social interaction tests. "Approach-Investigation" was defined as when the test animal walked directly towards the cupped animal, reached at least a quarter of body length away from the cup, and investigated it.

In social interaction and four-cup tests, the nose point, head, and body center of the test animal were tracked with custom DLC models [50]. In the social interaction test, the cage was evenly divided into 7 zones along the cage width, with zone 1 being the farthest from the cup side. We then calculated the percentage of time when the nose of the test animal was located in the far zone (zones 1–2). In the four-cup test, "Time around the cup" was defined as when the head of the test animal was within one body length away from the cup edge.

In the real-time place preference test, the animal was allowed to freely explore the test arena (two compartments, each compartment measured as 30 cm (L) × 20 cm (W) × 25 cm (H)) for 10 minutes without light stimulation. The compartment where the animal spent less time

was assigned as the stimulation compartment. Then the light was delivered to the test animal whenever it entered the stimulation compartment for 20 minutes. For analysis, we tracked the body center of the animal using a custom-built DLC model and calculated the percentage of time the body center was located in the stimulation compartment during baseline and light delivery periods.

### Fiber photometry recording

The fiber photometry setup was constructed as previously described [9,13,51,52]. Briefly, a 390-Hz sinusoidal blue LED light (30 μW) (LED light: M470F1; LED driver: LEDD1B; both from Thorlabs) was band-pass filtered (passing band: 472 ± 15 nm; FF02–472/30–25, Semrock) and delivered to the brain to excite GCaMP6f. The emission lights traveled back through the same optical fiber, were band-pass filtered (passing bands: 535 ± 25 nm; FF01–535/505, Semrock), passed through an adjustable zooming lens (SM1NR01, Thorlabs; Edmun optics no. 62–561), were detected by a Femtowatt Silicon Photoreceiver (Newport, 2151), and recorded using a real-time processor (RZ5, TDT). The envelope of the 390-Hz signals reflected the intensity of GCaMP6f and was extracted in real-time using a custom TDT OpenEX program. The signal was low-pass filtered with a cut-off frequency of 5 Hz.

For fiber photometry recording of $VMHvl^{Esr1}$ cells during $MPOA^{Esr1}$ cell activation and inactivation, aggressive adult male $Esr1^{Cre}$ mice were selected for surgery. The mice were injected with either AAV2-hSyn-DIO-hM3Dq-mCherry, AAV8-hSyn-DIO-hM4Di-mCherry, or AAV2-hSyn-DIO-mCherry (control group) bilaterally into the MPOA, and AAV2-CAG-Flex-GCaMP6f-WPRE-SV40 into the VMHvl unilaterally. Three weeks after surgery, the mice were further trained in an R-I test for 3 to 7 days to ensure high and stable aggression (attack consistently with latency to first attack <2 mins for 3 consecutive days). During recording, the test mouse first freely moved in its home cage for 30 min (baseline) and then received an intraperitoneal injection of saline. On the next day, we repeated the recording procedure, but instead of saline, we injected 1mg/kg CNO. The recording continued for 40 minutes after saline or CNO injection.

For fiber photometry recording of the $rMPOA^{Esr1}$ and $cMPOA^{Esr1}$ cells in Figure 1, three weeks after virus injection and on the day of recording, a Balb/C male intruder and then a C57BL/6 female intruder was introduced into the home cage of the recording mouse, each for 10 minutes, with 10–20 minutes in between. For recording shown in Figure 2, three weeks after surgery, the recording mouse was habituated in the test arena (45 cm × 45 cm) with four empty cups for 20 minutes/day for two days. On the recording day, the animal freely explored the test chamber that contained four cups, each placed in one corner of the test area, for 20 minutes. One cup was empty, and the remaining three others each contained a stimulus animal as described in “behavior tests and analysis”. The test mouse encountered none of the stimulus animals before the four-cup social interaction test. In each of the three days following the four-cup test, the recording mouse encountered the same Balb/C male for 10 minutes and then 5 minutes later, the same SW male aggressor for 10 minutes. On the next day, the recording animal went through a 20-min four-cup test again with the same set of stimulus animals.

For data analysis, we first used the MATLAB function ‘msbackadj’ with a moving window of 25% of the total recording duration to obtain the instantaneous baseline signal. The instantaneous ΔF/F value was calculated as $(F_{raw}-F_{baseline})/F_{baseline}$. For the $VMHvl^{Esr1}$ population recording, the $Ca^{2+}$ transients were detected using the MATLAB function “findpeaks” with a peak detection threshold of 0.02. The transient magnitude was calculated as the peak ΔF/F minus the preceding trough ΔF/F. The ratio of average transient magnitude and frequency between pre- and post-injection was then calculated and compared between saline and CNO groups. For the $MPOA^{Esr1}$ population recording, ΔF/F was first calculated as described above, and then Z scored. The PETHs of Z scored ΔF/F aligned to various behaviors were constructed for each animal and then averaged across animals. The response during a specific behavior for each animal was calculated by averaging the Z scored ΔF/F during all periods when the behavior occurred.

## Slice recording

Three weeks after virus injection, acute coronal brain slices containing VMHvl (275 μm in thickness) were collected using standard methods [13]. Isoflurane-anesthetized mice were perfused with an ice-cold choline-based cutting solution containing (in mM) 25 $NaHCO_3$,25 glucose, 1.25 $NaH_2PO_4$, 7 $MgCl_2$, 2.5 KCl, 0.5 $CaCl_2$, 110 choline chloride, 11.6 ascorbic acid, and 3.1 pyruvic acid. The slices were collected in the same cutting solution using a Leica VT1200s vibratome, incubated for 20 min in oxygenated artificial cerebrospinal fluid (ACSF) solution (in mM: 125 NaCl, 2.5 KCl, 1.25 $NaH_2PO_4$, 25 $NaHCO_3$, 1 $MgCl_2$, 2 $CaCl_2$, and 11 glucose) (osmolality, 295 mmol/kg) at 32– 34°C and then maintained at room temperature until use. Individual slices containing VMHvl were then transferred to a recording chamber and superfused with ACSF, warmed to 32– 34°C, and bubbled with 95% $O_2$ and 5% $CO_2$. mCherry labeled Esr1 cells within VMHvl from $Esr1^{Cre}$ mice, glutamatergic VMHvl cells (zsGreen positive cells from $Vglut2^{Cre}$ × Ai6 mice, and zsGreen negative cells from $Vgat^{Cre}$ × Ai6 mice) and GABAergic cells surrounding VMHvl (zsGreen negative cells from $Vglut2^{Cre}$ × Ai6 mice, and zsGreen positive cells from $Vga^{tCre}$ × Ai6 mice) were identified with an Olympus 40 × water-immersion objective with TXRED and GFP filters. Standard whole-cell recordings were performed with MultiClamp 700B amplifier (Molecular Devices) and Clampex 11.0 software (Axon Instruments). Membrane currents were low-pass filtered at 2 kHz and digitized at 10 kHz with Digidata 1550B (Axon Instruments). Electrode resistances were 2–4 MΩ, and most neurons had series resistance from 4 to 15 MΩ. The intracellular solution contained (in mM) 135 $CsMeSO_3$, 10 HEPES, 1 EGTA, 3.3 QX-314 ($Cl^-$ salt), 4 Mg-ATP, 0.3 Na-GTP, 8 $Na_2$-Phosphocreatine (osmolality, 295 mmol/kg; pH 7.3 adjusted with CsOH) and 0.2% biocytin (Tocris, 3349). To activate ChR2- or Chrimson-expressing axons in VMHvl, brief pulses of full-field illumination (1 ms × 5) generated by a 470 nm or 605 nm LED (pE-300white; CoolLED) were delivered onto the recorded neuron at an interval of 35 s. Voltage clamp recording was conducted on $VMHvl^{Esr1}$ cells from $Esr1^{Cre}$ mice, putative $VMHvl^{Vglut2}$ cells, and $TU^{Vgat}$ cells from $Vglut2^{Cre}$ × Ai6 and $Vgat^{Cre}$ × Ai6 mice. The membrane voltage was held at −70 mV for oEPSC recording and at 0 mV for oIPSC recording. The locations of the recorded cells were further confirmed histologically by immunostaining of biocytin. The representative recording traces were plotted suing Origin 2018. Various measurements were obtained using Clampfit and analyzed using Prism.

### Anterograde and retrograde tracing

To investigate the downstream targets of the MPOA$^{Esr1}$ population, we collected the brains 2~3 weeks after viral injection for histological analysis. Every third section (50 μm thickness) was collected. For monosynaptic retrograde rabies tracing, brains were collected 5–7 days after rabies injection. All sections (30 μm) throughout MPOA and VMH[24] were collected. The collected brain sections were stained for DAPI (1:20,000; Thermo Fisher, D1306), mounted on Superfrost slides (Fisher Scientific, 12–550-15 or MAS-03, Matsunami), and coverslipped for imaging using a virtual slide scanner (Olympus, VS120).

ImageJ was used to analyze the density of MPOA$^{Esr1}$ cell projection. A small boxed area was selected in each of the regions of interest, and the average pixel intensity of the boxed area was calculated as $F_{raw}$. The sizes of the selected boxes are: 220 × 220 μm (LSv), 120 × 120 μm (PVN), 250 × 250 μm (RCh), 320 × 75 μm (Pv), 120 × 120 μm (ARH), 250 × 250 μm (DMH), 150 × 150 μm (VMHvl), 170 × 170 μm (TU), 220 × 220 μm (MeApd), 170 × 170 μm (PMv), 100 × 100 μm (PvP), 200 × 200 μm (PA), 220 × 220 μm (PAG), 190 × 400 μm (SUM), and 330 × 200 μm (VTA). On each image, a boxed area of the same size but in a brain region with no visible fiber terminals was selected for calculating the background intensity ($F_{background}$). $F_{signal}$ was calculated as $F_{raw}$ minus $F_{background}$. For each animal, $F_{signal}$ was normalized by the maximum $F_{signal}$ across all the analyzed regions. The normalized $F_{signal}$ was then used for calculating the average terminal field intensity across animals.

All retrogradely labeled cells in the MPOA and starter cells in VMHvl were counted using ImageJ. The number of MPOA cells at each Bregma level was then normalized by the total of VMHvl started cells in each animal and then averaged across animals.

### Immunohistochemistry

Fos staining was conducted as previously described[53]. Briefly, the mice were perfused transcardially with 0.1 M Phosphate-buffered Saline (1× PBS) followed by 4% paraformaldehyde (PFA) in 1 × PBS. The brains were extracted, post-fixed in 4% PFA for 2 ~ 3 hours at 4 °C followed by 48 hours in 30% sucrose, and then they were embedded in O.C.T. compound (Fisher Healthcare) and frozen on dry ice. 40 μm thick coronal brain sections were cut using a cryostat (model #CM3050S, Leica Biosystems) and collected in PBS. After that, the brain slices were washed with PBS (1 × 10 minutes) and blocked in PBS-T (0.3% Triton X-100 in 1× PBS) with 5% normal donkey serum (NDS, Jackson Immuno Research) for 30 minutes at room temperature. The slices were then incubated in primary antibody diluted in blocking solution (guinea pig anti-c-Fos, 1:2000, Synaptic Systems, 226–005, Lot #2–10, 2–13) at 4 °C for 16 – 20 hours, washed with PBS-T (3 × 10 minutes), incubated in secondary antibody diluted in 5% NDS containing PBS-T (Alexa Fluor 488-conjugated goat anti-guinea pig IgG, 1:500, Invitrogen. #A11073, lot#2160428) for 4 hours, washed with PBS-T (2 × 10 minutes) and then stained with DAPI (1:10000, Thermo Scientific) for 20 minutes. Slides were coverslipped using a mounting medium (Fluoromount, Diagnostic BioSystems, #K024) after drying. The 10× fluorescent images of all brain sections were acquired using Olympus VS120 Automated Slide Scanner. Cells

in the rMPOA and cMPOA were counted using Adobe photoshop 2020 (Adobe). For representative images, 20× fluorescent confocal images were acquired (Zeiss LSM 800).

After patch clamp recording, the recorded brained slice was transferred to 4% PFA for 30 ~ 60 minutes, washed with PBS (3 × 10 minutes), and incubated with pacific blue-conjugated streptavidin (1:250; Thermo Fisher, S11222) containing 10% donkey serum PBS-T (0.3% Triton-× 100 in 1 × PBS) overnight at 4 °C. The next morning, the slices were washed with PBS (3 ×10 minutes), incubated with Topro-3 (1:2000; Thermo Fisher, T3605) for 20 minutes at room temperature, washed with PBS, mounted on SuperFrost slides (Fisher Scientific, 12–550-15), and coverslipped for imaging on a confocal microscope (Zeiss LSM 510 or 700 microscope).

## Statistics and Reproducibility

No statistical methods were used to pre-determine sample sizes but our sample sizes are similar to those reported in previous publications[13,24,25,52,54]. All experiments were conducted using 2 to 4 cohorts of animals. The results were reproducible across cohorts and combined for final analysis. All statistical analyses were performed using MATLAB or Prism software. All statistical analyses were two-tailed. Parametric tests, including two-tailed paired t-tests and two-tailed unpaired t-tests, were used if distributions passed Kolmogorov–Smirnov or Shapiro-Wilk tests for normality or else nonparametric tests, including two-tailed Wilcoxon matched-pairs signed rank test and two-tailed Mann Whitney test, were used. For comparisons across multiple groups and variables, Two-way ANOVA with repeated measures was used without formally testing the normality of data distribution. Followed Two-way ANOVA, differences between groups were assessed using Sidak's multiple comparison test or Tukey's multiple comparisons test. Two-sided Fisher's exact test and two-sided McNemar's test were used to determine whether the proportions of categories in two independent and dependent groups differ from each other, respectively. All p values < 0.1 were indicated in the figures. *p< 0.05; **p<0.01; ***p<0.001; ****p<0.0001. Error bars represent ± SEM. For detailed statistical results, see the source data file associated with each figure.

## Extended Data

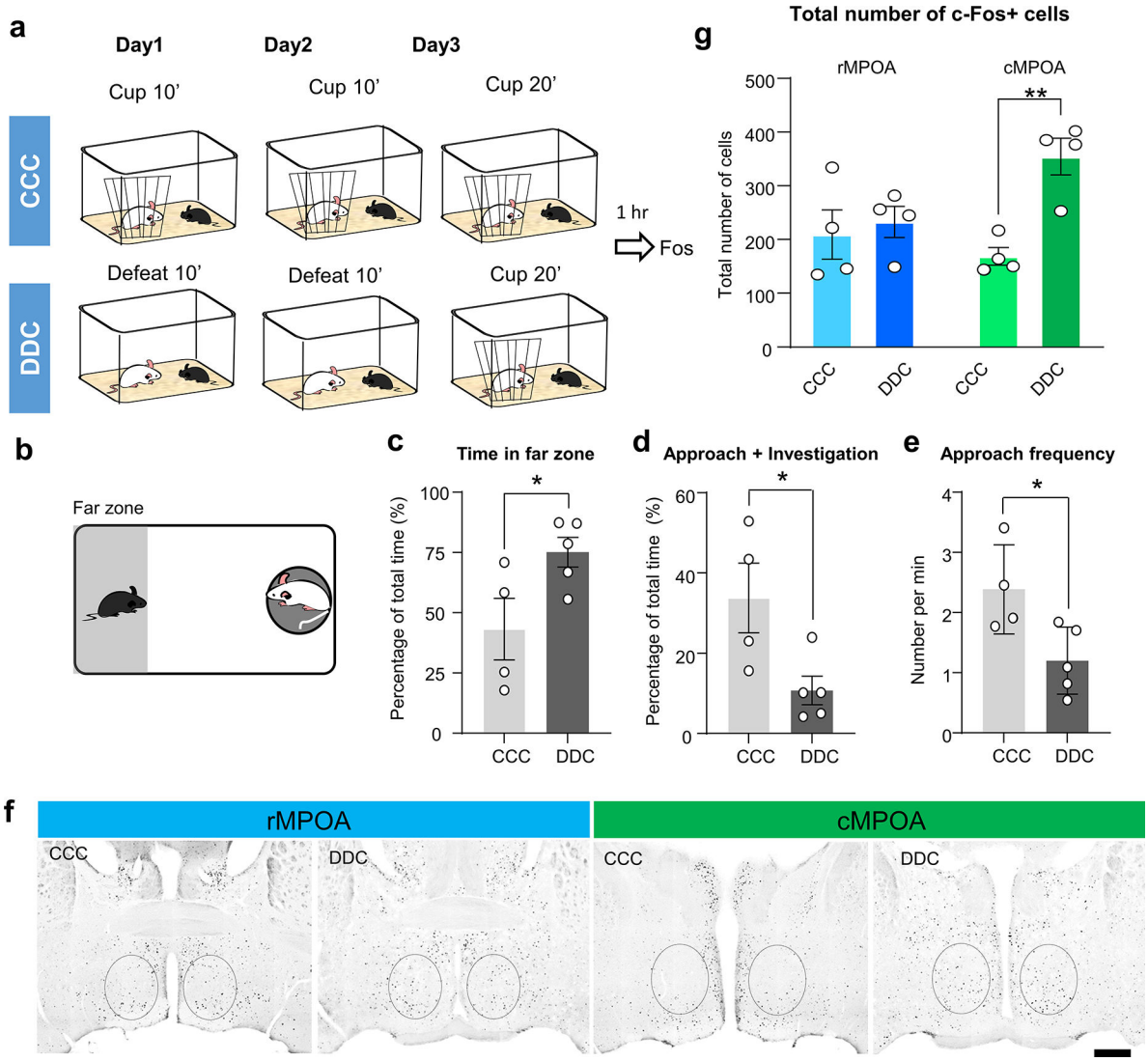


**Extended Data Fig. 1. cMPOA in males show higher aggressor cue-induced c-Fos after defeat.**

**(a)**, Schematic illustration of the experimental procedures. CCC: cup-cup-cup; DDC: defeat-defeat-cup. **(b)**, Schematic illustration of the cup assay performed on the third day. **(c)**, Percentage of time the animal spent in far zone, as illustrated in **(b)**. **(d)**, Percentage of time the animal spent on approaching and investigating the cupped aggressor. **(e)**, Frequency of approach toward the cupped aggressor. **(f)**, Representative images showing c-Fos expressing cells in rMPOA and cMPOA after CCC and DDC tests. Scale bar, 0.5 mm. **(g)**, Quantification of c-Fos-positive cells in the rMPOA and cMPOA in CCC and DDC groups. Four sections were counted for each MPOA sub-region for each animal. All data are presented as mean ± s.e.m. **(c–e)**, $n = 4$ mice for CCC group, and 5 mice for DDC group. **(g)**, $n = 4$ mice per group. Two-tailed paired $t$-test; $^{*}P < 0.05$; $^{**}P < 0.01$; Otherwise, $P > 0.05$.

| | Resident | Intruder | Resident win | Tie | NF | Intruder win | Resident RHP | Intruder RHP | Average RHP |
|---|---|---|---|---|---|---|---|---|---|
| SW SH vs. C57 SH | SW SH | C57 SH | 202 | 0 | 0 | 0 | 1 | 0 | SW SH: 0.94 |
| | C57 SH | SW SH | 5 | 6 | 0 | 59 | 0.11 | 0.89 | C57 SH: 0.06 |
| C57 SH vs. BC GH | C57 SH | BC GH | 340 | 0 | 266 | 0 | 0.78 | 0.22 | C57 SH: 0.73 |
| | BC GH | C57 SH | 0 | | 20 | 12 | 0.31 | 0.69 | BC GH: 0.27 |
| SW SH vs. BC GH | SW SH | BC GH | 20 | 0 | 0 | 0 | 1 | 0 | SW SH: 1 |
| | BC GH | SW SH | 0 | 0 | 0 | 21 | 0 | 1 | BC GH: 0 |

$$RHP = \frac{(\#win \times 1 + \#tie \times 0.5 + \#NF \times 0.5 + \#lose \times 0)}{(\#win + \#tie + \#NF + \#lose)}$$

NF: No fight; SH: single-housed; GH: group-housed.

**Extended Data Fig. 2. RHP of each animal in pairs of male mice with different genetic backgrounds.**

SW test males are single-housed, sexually experienced and with repeated winning experience. C57 test males are single-housed, sexually naive and with no or one-time winning experience. BC test males are group-housed, sexually naive and with no winning experience.

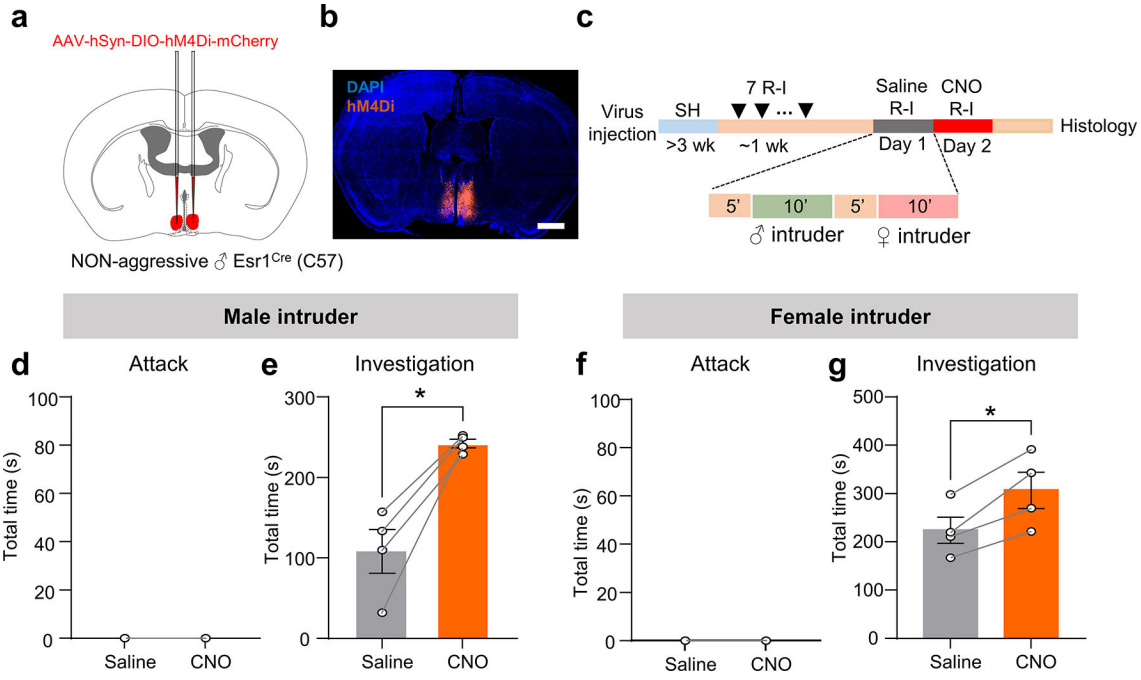


**Extended Data Fig. 3. Inhibiting cMPOA$^{Esr1}$ cells does not elicit aggression in non-aggressive male mice.**

**(a)** Viral strategy for chemogenetic inhibition of cMPOA$^{Esr1}$ cells in non-aggressive male mice. **(b)** A representative histology image ($n = 4$ mice) showing the expression of hM4Di-mchery in cMPOA$^{Esr1}$ cells. Scale bar, 1 mm. **(c)** Experimental timeline. **(d,f)** hM4Di test male mice showed no attack toward a male intruder **(d)** or a female intruder **(f)** after saline or CNO injection. **(e,g)** Investigation duration toward a male intruder **(e)** or a female intruder **(g)** increased after CNO injection in comparison to saline injection in hM4Di non-aggressive male mice. All data are presented as mean ± s.e.m. $n = 4$ mice. Two-tailed paired $t$-test **(e and g)**; $^*P < 0.05$.

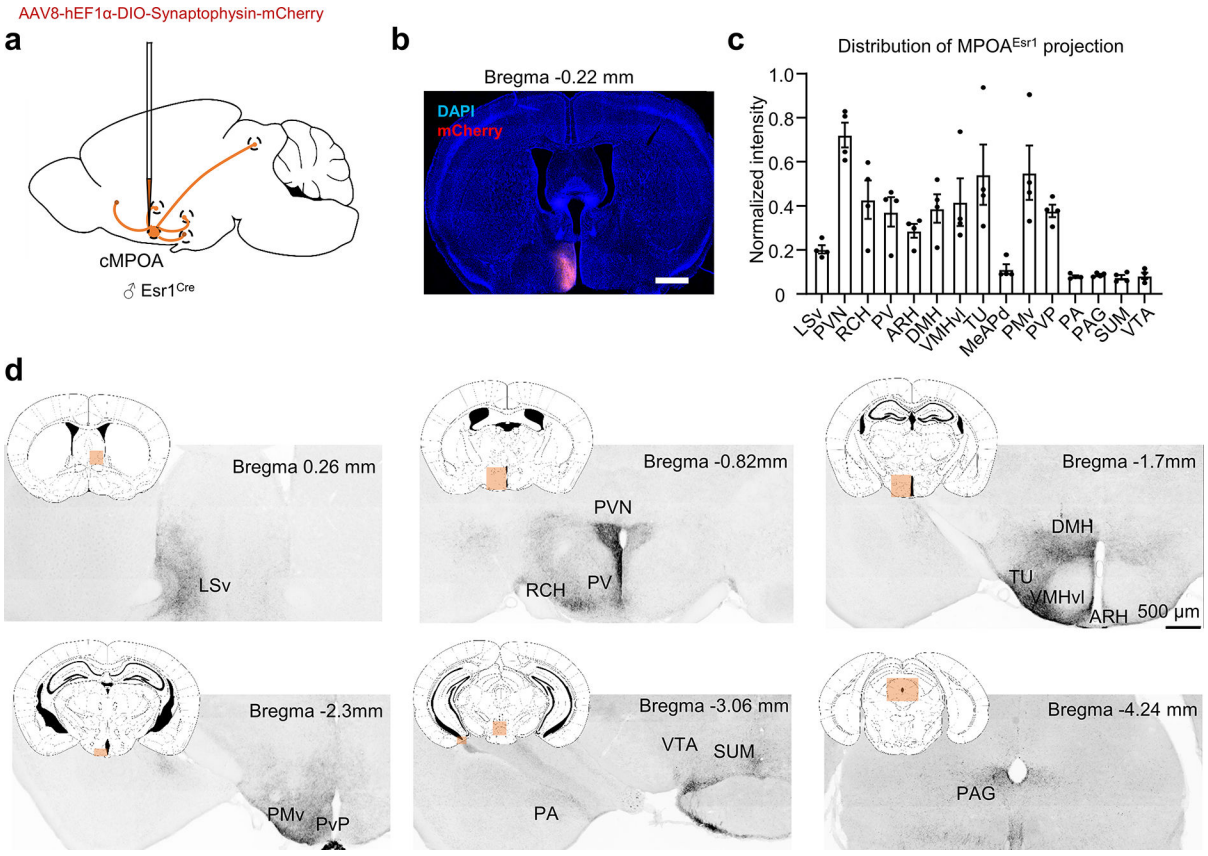


**Extended Data Fig. 4. Projection pattern of cMPOA$^{Esr1}$ cells in male mice.**

**(a)** Viral strategy for expressing Synaptophysin-mCherry in cMPOA$^{Esr1}$ cells. **(b)** A representative histology image showing the expression of Synaptophysin-mCherry in MPOA$^{Esr1}$ cells. Scale bar, 1 mm. **(c)** Quantification of Synaptophysin-mCherry signal in various regions across the brain. For each animal, intensity in each region is normalized by the highest intensity among all regions. **(d)** Representative images showing Synaptophysin-mCherry signal in various brain regions of a male mouse. LSv, lateral septum ventral part; PVN, paraventricular nucleus of the hypothalamus; RCH, retrochiasmatic area; PV, periventricular hypothalamic nucleus; ARH, Arcuate hypothalamic nucleus; DMH, dorsomedial hypothalamic nucleus; VMHvl, ventromedial hypothalamus ventrolateral part; TU, tuberal nucleus; MeAPd, medial amygdala nucleus posterodorsal part; PMv, ventral premammillary nucleus; PVP, periventricular hypothalamic nucleus, posterior part; PA, posterior amygdala; PAG, periaqueductal gray; SUM, supramammillary nucleus; VTA, ventral tegmental area. All data are presented as mean ± s.e.m. $n$ = 4 mice.

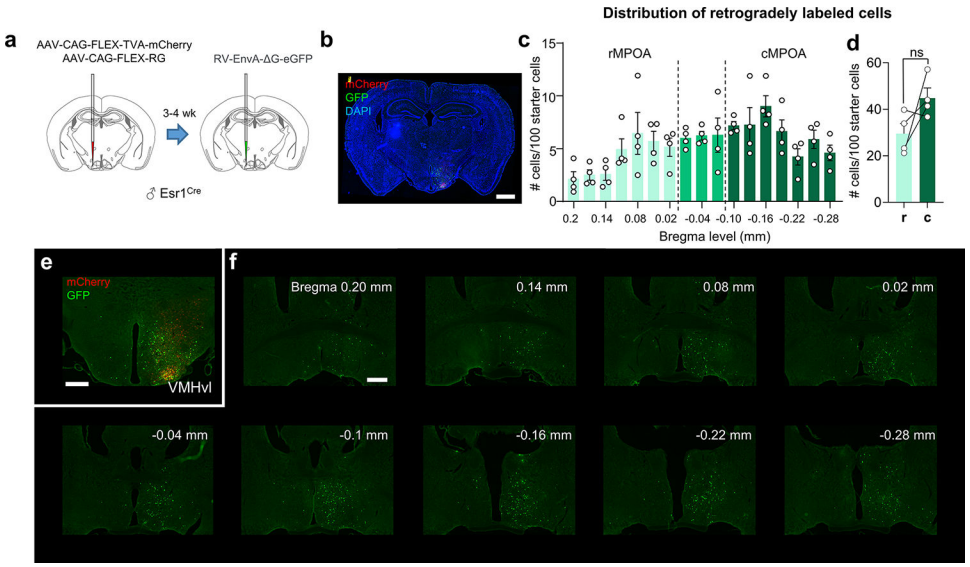


**Extended Data Fig. 5. Monosynaptic rabies tracing reveals strong inputs from both rostral and caudal MPOA to VMHvl$^{Esr1}$ cells.**

**(a)** Schematic illustration of viral injections for monosynaptic rabies tracing. All viruses were injected unilaterally. **(b)** A representative image showing expression of mCherry (red) and GFP (green) in the VMHvl. Scale bar, 1 mm. **(c)** Number of GFP-positive cells per 100 starter cells in the VMHvl in the MPOA on each 30 μm section along the anterior–posterior axis. **(d)** The total number of GFP-positive cells in the rMPOA (r) and cMPOA (c). The GFP cell number is normalized by the starter cell number in the VMHvl. Two-tailed paired *t*-test. ns: $P > 0.05$. **(e)** A representative image showing starter cells that express both mCherry (red) and GFP (green) in the VMHvl. Scale bar, 0.5 mm. **(f)** Representative images showing GFP cells in the MPOA from Bregma level 0.2 mm to −0.28 mm. Scale bar, 0.5 mm. All data are presented as mean ± s.e.m. **(c**,**d)**, $n = 4$ mice.

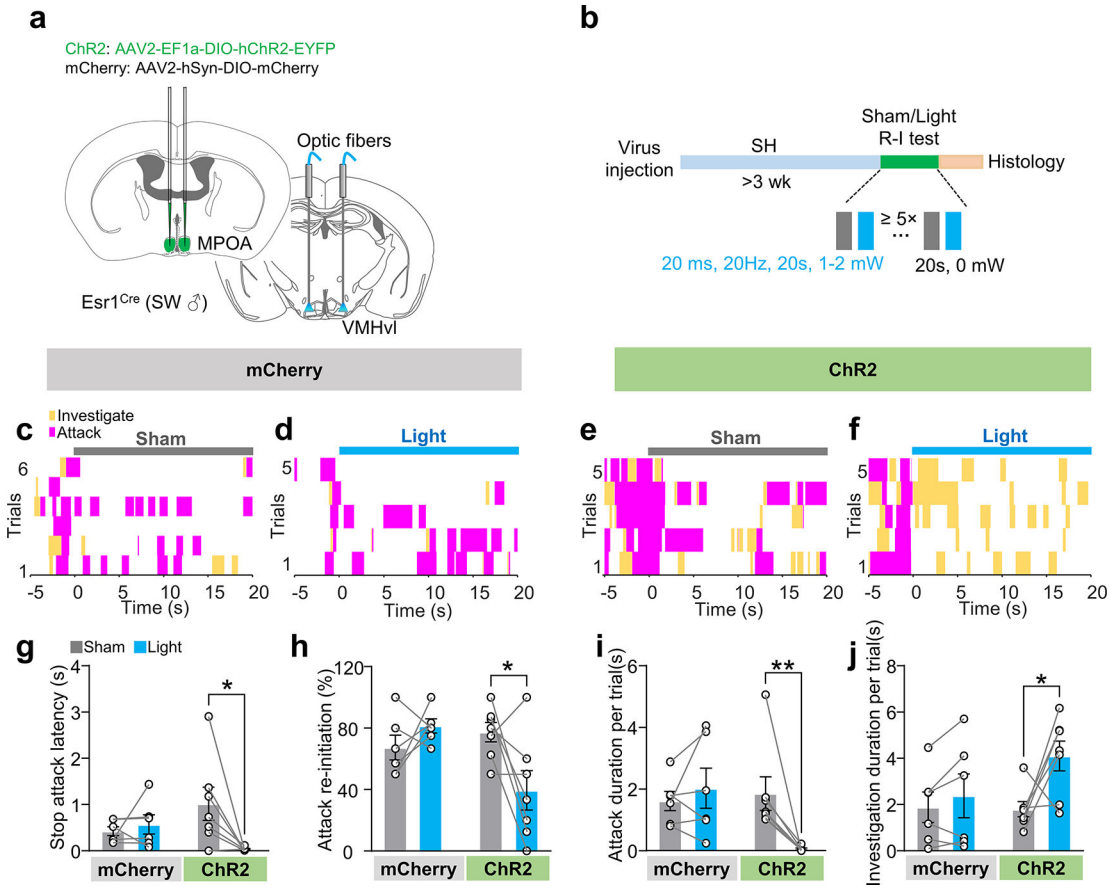


**Extended Data Fig. 6. Optogenetic activation of cMPOA$^{Esr1}$-VMHvl pathway suppresses attack in naive SW males.**

**(a)** Viral strategy for optogenetic activation of cMPOA$^{Esr1}$-VMHvl terminals in naive SW males. **(b)** Experimental timeline. **(c,d)** Representative raster plots showing attack and investigation toward a male intruder in mCherry control mice aligned to sham **(c)** and light **(d)** onsets. **(e,f)** Representative raster plots from a ChR2 test mouse. **(g-j)** The stop attack latency **(g)**, attack re-initiation probability **(h)**, attack duration per trial **(i)**, and investigation duration per trial **(j)** toward a C57 male intruder during sham and light stimulation of mCherry control and ChR2 test SW mice. All data are presented as mean ± s.e.m. $n = 6$ mice for mCherry group and 7 mice for ChR2 group. Two-way RM ANOVA with Sidak's multiple comparisons test **(g-j)**; $*P < 0.05$; $**P < 0.01$; Otherwise, $P > 0.05$.

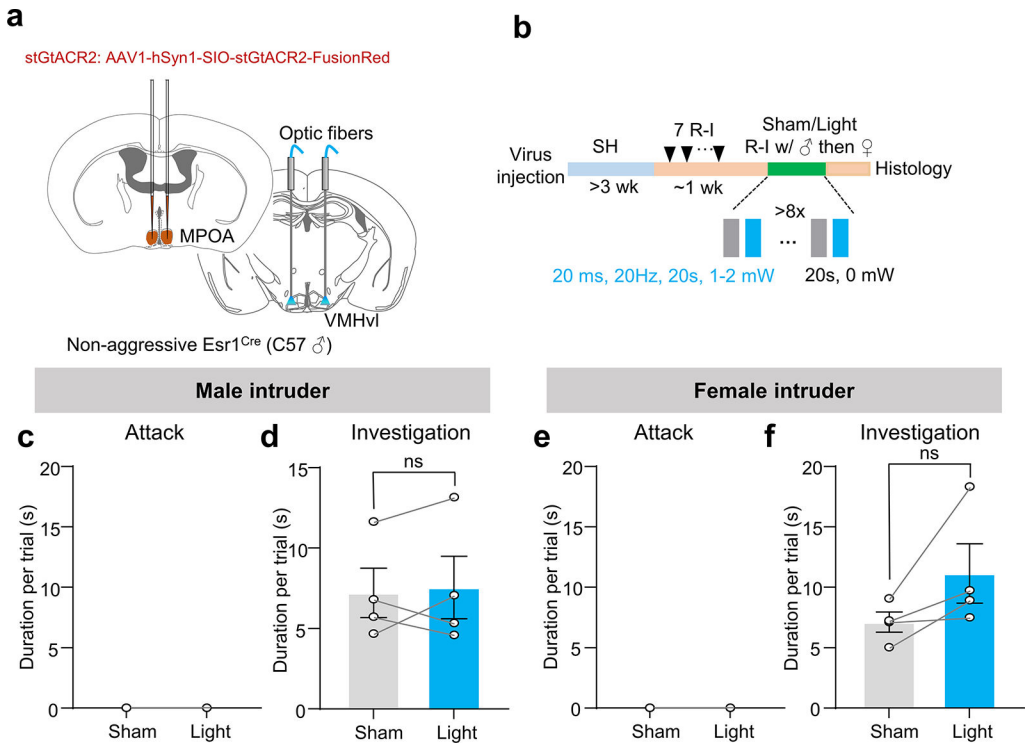


**Extended Data Fig. 7. Optogenetic inactivation of cMPOA$^{Esr1}$-VMHvl projection does not induce attack in non-aggressive male mice.**

**(a)** Viral strategy for optogenetic inactivation of cMPOA$^{Esr1}$-VMHvl terminals. **(b)** Experimental timeline. **(c,d)** The average attack duration **(c)** and investigation duration **(d)** toward a male intruder during each 20 s sham and light stimulation in stGtACR2 non-aggressive male mice. **(e,f)** The average attack duration **(e)** and investigation duration **(f)** toward a female intruder during each 20 s sham and light stimulation in stGtACR2 non-aggressive male mice. All data are presented as mean ± s.e.m. $n = 4$ mice. **(d and f)** Two-tailed paired $t$-test. All $P > 0.05$.

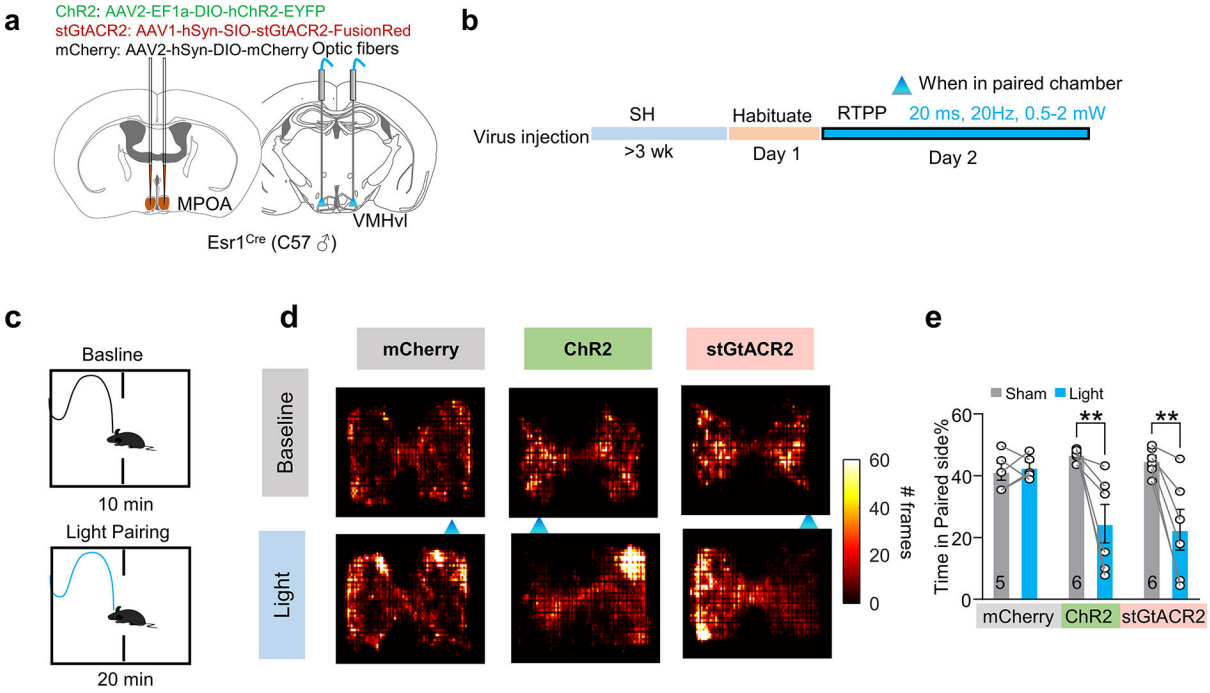


**Extended Data Fig. 8. Optogenetic activation or inhibition of cMPOA$^{Esr1}$-VMHvl terminals is aversive.**

**(a)** Virus injection and fiber placement for cMPOA$^{Esr1}$-VMHvl terminal manipulation. **(b)** Experimental timeline. **(c)** Schematics for RTPP test. **(d)** Heatmaps showing the body center location of the test mouse before and during light pairing. Blue triangles indicate light-paired chambers. **(e)** Percentage of time spent in light-paired chamber at the baseline and during light stimulation periods. All data are presented as mean ± s.e.m. $n = 5$ mice for mCherry group, 6 mice for ChR2 group, and 6 mice for stGtACR2 group. Two-way RM ANOVA with Sidak's multiple comparisons test. $^{**}P < 0.01$; Otherwise, $P > 0.05$.

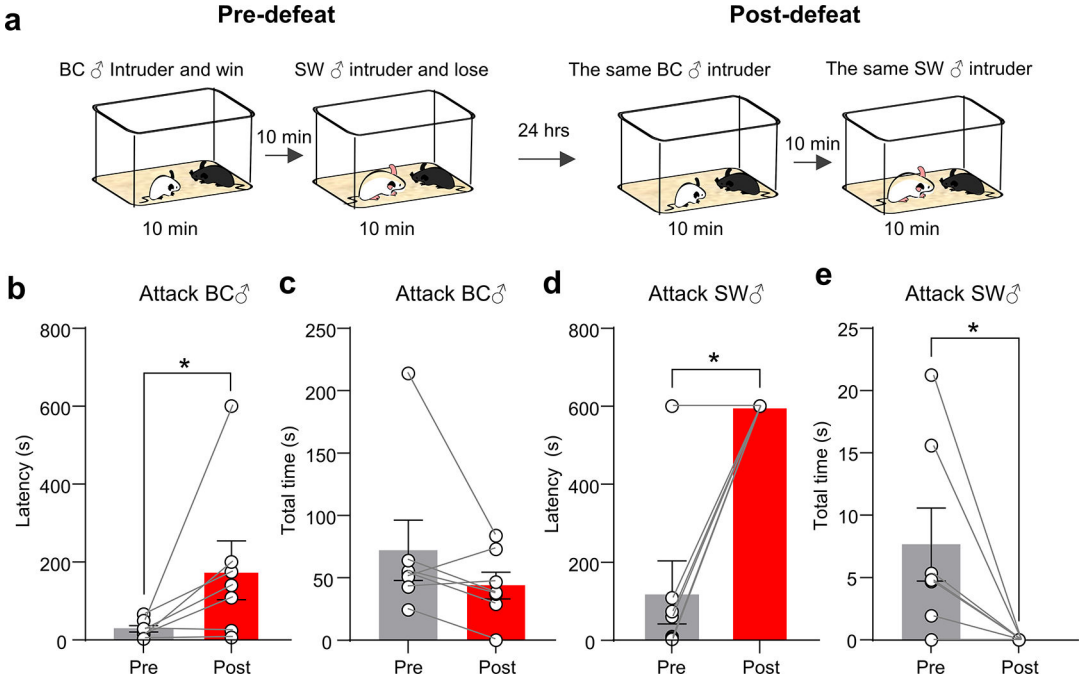


**Extended Data Fig. 9. One-time defeat strongly suppresses aggression of the loser toward the winner.**

**(a)** Schematic illustration of the assays. **(b,c)** Latency to attack a non-aggressive BC male intruder **(b)** and the total duration of attack **(c)** before and after defeat by the SW aggressor. **(d,e)** Latency to attack an aggressive SW male intruder **(d)** and the total duration of attack **(e)** before and after defeat by the same SW aggressor. All data are presented as mean ± s.e.m. **(b-e)**, $n = 7$ mice. Two-tailed paired $t$-test; $^*P < 0.05$; Otherwise, $P > 0.05$.

## Acknowledgements

We thank Lynn Shan and Christopher Richter for help with behavior annotation, and Luping Yin for providing some MATLAB codes for analysis. This research was supported by NIH grants R01MH101377, R01MH124927, 1R01HD092596 and U19NS107616 (D.L.); the Mathers Foundation, and the Vulnerable Brain Project (D.L.); the Uehara Memorial Foundation, JSPS Overseas Research Fellowship and Osamu Hayaishi Memorial Scholarship (T.O.); and the Sumitomo Foundation (T.Y.)

## Data availability

Raw values associated with each figure panel can be found in the source data files. Fiber photometry recording data, behavior annotations and raw representative histology images can be downloaded from 10.5281/zenodo.7700343. Behavior videos and additional histology images are available from the corresponding author upon reasonable request.

## References

1. Parker GA Assessment strategy and the evolution of fighting behaviour. J Theor Biol 47, 223–243, doi:10.1016/0022-5193(74)90111-8 (1974). [PubMed: 4477626]
2. Lischinsky JE & Lin D Neural mechanisms of aggression across species. Nat Neurosci 23, 1317–1328, doi:10.1038/s41593-020-00715-2 (2020). [PubMed: 33046890]

3. Zha X & Xu X-H Neural circuit mechanisms that govern inter-male attack in mice. Cellular Molecular Life Sciences 78, 7289–7307 (2021). [PubMed: 34687319]
4. Nelson RJ & Trainor BC Neural mechanisms of aggression. Nat Rev Neurosci 8, 536–546, doi:10.1038/nrn2174 (2007). [PubMed: 17585306]
5. Hashikawa K, Hashikawa Y, Falkner A & Lin D The neural circuits of mating and fighting in male mice. Curr Opin Neurobiol 38, 27–37, doi:10.1016/j.conb.2016.01.006 (2016). [PubMed: 26849838]
6. Lee H et al. Scalable control of mounting and attack by Esr1+ neurons in the ventromedial hypothalamus. Nature 509, 627–632, doi:10.1038/nature13169 (2014). [PubMed: 24739975]
7. Lin D et al. Functional identification of an aggression locus in the mouse hypothalamus. Nature 470, 221–226, doi:10.1038/nature09736 (2011). [PubMed: 21307935]
8. Yang CF et al. Sexually dimorphic neurons in the ventromedial hypothalamus govern mating in both sexes and aggression in males. Cell 153, 896–909, doi:10.1016/j.cell.2013.04.017 (2013). [PubMed: 23663785]
9. Falkner AL, Grosenick L, Davidson TJ, Deisseroth K & Lin D Hypothalamic control of male aggression-seeking behavior. Nat Neurosci 19, 596–604, doi:10.1038/nn.4264 (2016). [PubMed: 26950005]
10. Yang T et al. Social Control of Hypothalamus-Mediated Male Aggression. Neuron 95, 955–970 e954, doi:10.1016/j.neuron.2017.06.046 (2017). [PubMed: 28757304]
11. Lo L et al. Connectional architecture of a mouse hypothalamic circuit node controlling social behavior. Proc Natl Acad Sci U S A 116, 7503–7512, doi:10.1073/pnas.1817503116 (2019). [PubMed: 30898882]
12. Wei Y-C et al. Medial preoptic area in mice is capable of mediating sexually dimorphic behaviors regardless of gender. Nature communications 9, 1–15 (2018).
13. Fang YY, Yamaguchi T, Song SC, Tritsch NX & Lin D A Hypothalamic Midbrain Pathway Essential for Driving Maternal Behaviors. Neuron 98, 192–207 e110, doi:10.1016/j.neuron.2018.02.019 (2018). [PubMed: 29621487]
14. Karigo T et al. Distinct hypothalamic control of same- and opposite-sex mounting behaviour in mice. Nature 589, 258–263, doi:10.1038/s41586-020-2995-0 (2021). [PubMed: 33268894]
15. Bermond B Effects of medial preoptic hypothalamus anterior lesions on three kinds of behavior in the rat: Intermale aggressive, male-sexual, and mouse-killing behavior. Aggressive Behavior 8, 335–354 (1982).
16. Albert DJ, Walsh ML, Gorzalka BB, Mendelson S & Zalys C Intermale social aggression: suppression by medial preoptic area lesions. Physiol Behav 38, 169–173, doi:10.1016/0031-9384(86)90151-4 (1986). [PubMed: 3797483]
17. Edwards DA, Nahai FR & Wright P Pathways linking the olfactory bulbs with the medial preoptic anterior hypothalamus are important for intermale aggression in mice. Physiol Behav 53, 611–615, doi:10.1016/0031-9384(93)90162-9 (1993). [PubMed: 8451331]
18. Hammond MA & Rowe FA Medial preoptic and anterior hypothalamic lesions: influences on aggressive behavior in female hamsters. Physiol Behav 17, 507–513, doi:10.1016/0031-9384(76)90115-3 (1976). [PubMed: 1034941]
19. Sano K, Tsuda MC, Musatov S, Sakamoto T & Ogawa S Differential effects of site-specific knockdown of estrogen receptor alpha in the medial amygdala, medial pre-optic area, and ventromedial nucleus of the hypothalamus on sexual and aggressive behavior of male mice. Eur J Neurosci 37, 1308–1319, doi:10.1111/ejn.12131 (2013). [PubMed: 23347260]
20. Veening JG et al. Do similar neural systems subserve aggressive and sexual behaviour in male rats? Insights from c-Fos and pharmacological studies. Eur J Pharmacol 526, 226–239, doi:10.1016/j.ejphar.2005.09.041 (2005). [PubMed: 16263109]
21. Hashikawa Y, Hashikawa K, Falkner AL & Lin D Ventromedial Hypothalamus and the Generation of Aggression. Front Syst Neurosci 11, 94, doi:10.3389/fnsys.2017.00094 (2017). [PubMed: 29375329]
22. Knoedler JR et al. A functional cellular framework for sex and estrous cycle-dependent gene expression and behavior. Cell 185, 654–671 e622, doi:10.1016/j.cell.2021.12.031 (2022). [PubMed: 35065713]

23. Kim DW et al. Multimodal Analysis of Cell Types in a Hypothalamic Node Controlling Social Behavior. Cell 179, 713–728 e717, doi:10.1016/j.cell.2019.09.020 (2019). [PubMed: 31626771]
24. Wong LC et al. Effective Modulation of Male Aggression through Lateral Septum to Medial Hypothalamus Projection. Curr Biol 26, 593–604, doi:10.1016/j.cub.2015.12.065 (2016). [PubMed: 26877081]
25. Yin L et al. VMHvll(Cckar) cells dynamically control female sexual behaviors over the reproductive cycle. Neuron, doi:10.1016/j.neuron.2022.06.026 (2022).
26. Mitra SW et al. Immunolocalization of estrogen receptor beta in the mouse brain: comparison with estrogen receptor alpha. Endocrinology 144, 2055–2067, doi:10.1210/en.2002-221069 (2003). [PubMed: 12697714]
27. Moffitt JR et al. Molecular, spatial, and functional single-cell profiling of the hypothalamic preoptic region. Science 362, doi:10.1126/science.aau5324 (2018).
28. Tsuneoka Y et al. Functional, anatomical, and neurochemical differentiation of medial preoptic area subregions in relation to maternal behavior in the mouse. J Comp Neurol 521, 1633–1663, doi:10.1002/cne.23251 (2013). [PubMed: 23124836]
29. Simerly RB & Swanson LW The organization of neural inputs to the medial preoptic nucleus of the rat. J Comp Neurol 246, 312–342, doi:10.1002/cne.902460304 (1986). [PubMed: 3517086]
30. Simerly RB & Swanson LW Projections of the medial preoptic nucleus: a Phaseolus vulgaris leucoagglutinin anterograde tract-tracing study in the rat. J Comp Neurol 270, 209–242, doi:10.1002/cne.902700205 (1988). [PubMed: 3259955]
31. Stagkourakis S et al. A neural network for intermale aggression to establish social hierarchy. Nature neuroscience 21, 834–842 (2018). [PubMed: 29802391]
32. Chen AX et al. Specific Hypothalamic Neurons Required for Sensing Conspecific Male Cues Relevant to Inter-male Aggression. Neuron 108, 763–774 e766, doi:10.1016/j.neuron.2020.08.025 (2020). [PubMed: 32961129]
33. Motta SC et al. Ventral premammillary nucleus as a critical sensory relay to the maternal aggression network. Proceedings of the National Academy of Sciences 110, 14438–14443 (2013).
34. Soden ME et al. Genetic isolation of hypothalamic neurons that regulate context-specific male social behavior. Cell reports 16, 304–313 (2016). [PubMed: 27346361]
35. Bayless DW et al. Limbic Neurons Shape Sex Recognition and Social Behavior in Sexually Naive Males. Cell 176, 1190–1205 e1120, doi:10.1016/j.cell.2018.12.041 (2019). [PubMed: 30712868]
36. Yang B, Karigo T & Anderson DJ Transformations of neural representations in a social behaviour network. Nature 608, 741–749, doi:10.1038/s41586-022-05057-6 (2022). [PubMed: 35922505]
37. Dong HW & Swanson LW Projections from bed nuclei of the stria terminalis, posterior division: implications for cerebral hemisphere regulation of defensive and reproductive behaviors. Journal of Comparative Neurology 471, 396–433 (2004). [PubMed: 15022261]
38. Newman SW The medial extended amygdala in male reproductive behavior. A node in the mammalian social behavior network. Ann N Y Acad Sci 877, 242–257, doi:10.1111/j.1749-6632.1999.tb09271.x (1999). [PubMed: 10415653]
39. Stagkourakis S, Spigolon G, Liu G & Anderson DJ Experience-dependent plasticity in an innate social behavior is mediated by hypothalamic LTP. Proc Natl Acad Sci U S A 117, 25789–25799, doi:10.1073/pnas.2011782117 (2020). [PubMed: 32973099]
40. Harvey S, Jemiolo B & Novotny M Pattern of volatile compounds in dominant and subordinate male mouse urine. J Chem Ecol 15, 2061–2072, doi:10.1007/BF01207438 (1989). [PubMed: 24272296]
41. Hilakivi-Clarke LA & Lister RG The role of body weight in resident-intruder aggression. Aggressive Behavior 18, 281–287 (1992).
42. Diaz V & Lin D Neural circuits for coping with social defeat. Curr Opin Neurobiol 60, 99–107, doi:10.1016/j.conb.2019.11.016 (2020). [PubMed: 31837481]
43. Kollack-Walker S, Watson S & Akil H Social stress in hamsters: defeat activates specific neurocircuits within the brain. Journal of Neuroscience 17, 8842–8855 (1997). [PubMed: 9348352]
44. Motta SC & Canteras NS Restraint stress and social defeat: What they have in common. Physiol Behav 146, 105–110, doi:10.1016/j.physbeh.2015.03.017 (2015). [PubMed: 26066716]

45. Lkhagvasuren B et al. Distribution of Fos-immunoreactive cells in rat forebrain and midbrain following social defeat stress and diazepam treatment. Neuroscience 272, 34–57, doi:10.1016/j.neuroscience.2014.04.047 (2014). [PubMed: 24797330]

46. Remedios R et al. Social behaviour shapes hypothalamic neural ensemble representations of conspecific sex. Nature 550, 388–392, doi:10.1038/nature23885 (2017). [PubMed: 29052632]

47. Nordman JC et al. Potentiation of Divergent Medial Amygdala Pathways Drives Experience-Dependent Aggression Escalation. J Neurosci 40, 4858–4880, doi:10.1523/JNEUROSCI.0370-20.2020 (2020). [PubMed: 32424020]

## Method-only References:

48. Vong L et al. Leptin action on GABAergic neurons prevents obesity and reduces inhibitory tone to POMC neurons. Neuron 71, 142–154, doi:10.1016/j.neuron.2011.05.028 (2011). [PubMed: 21745644]

49. Madisen L et al. A robust and high-throughput Cre reporting and characterization system for the whole mouse brain. Nat Neurosci 13, 133–140, doi:10.1038/nn.2467 (2010). [PubMed: 20023653]

50. Mathis A et al. DeepLabCut: markerless pose estimation of user-defined body parts with deep learning. Nat Neurosci 21, 1281–1289, doi:10.1038/s41593-018-0209-y (2018). [PubMed: 30127430]

51. Hashikawa K et al. Esr1(+) cells in the ventromedial hypothalamus control female aggression. Nat Neurosci 20, 1580–1590, doi:10.1038/nn.4644 (2017). [PubMed: 28920934]

52. Yamaguchi T et al. Posterior amygdala regulates sexual and aggressive behaviors in male mice. Nat Neurosci 23, 1111–1124, doi:10.1038/s41593-020-0675-x (2020). [PubMed: 32719562]

53. Wang L et al. Hypothalamic Control of Conspecific Self-Defense. Cell Rep 26, 1747–1758 e1745, doi:10.1016/j.celrep.2019.01.078 (2019). [PubMed: 30759387]

54. Falkner AL et al. Hierarchical Representations of Aggression in a Hypothalamic-Midbrain Circuit. Neuron 106, 637–648 e636, doi:10.1016/j.neuron.2020.02.014 (2020). [PubMed: 32164875]

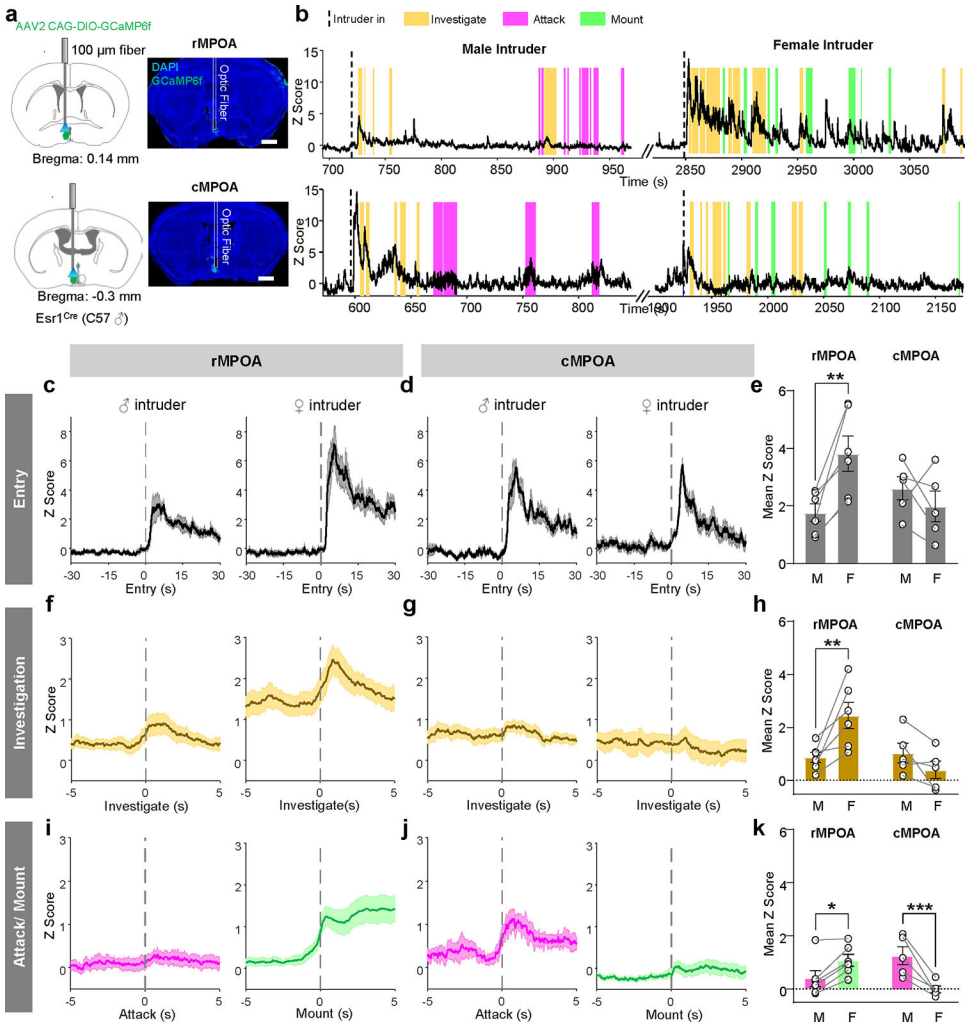


**Figure 1: Rostral and caudal MOPA$^{Esr1}$ cells show differential responses during social behaviors.**

**(a)** Viral strategy for GCaM6f expression in rMPOA$^{Esr1}$ (top left) and cMPOA$^{Esr1}$ cells (bottom left), and representative histology images showing the expression of GCaM6f in rMPOA$^{Esr1}$ (top right) and cMPOA$^{Esr1}$ cells (bottom right). Scale bars: 1 mm.

**(b)** Representative GCaMP6f recording traces (Z scored ΔF/F) of rMPOA$^{Esr1}$ cells (top) and cMPOA$^{Esr1}$ cells (bottom) during interaction with a male intruder (left) and a female intruder (right).

**(c-d)** Average post-event histograms (PETHs) of GCaMP6f signals of rMPOA$^{Esr1}$ **(c)** and cMPOA$^{Esr1}$ **(d)** cells aligned to the introduction of a male or a female intruder.

**(e)** Mean GCaMP6f signals during the first 30s after introduction of a male or a female intruder.

**(f-g)** Average PETHs of GCaMP6f signals of rMPOA$^{Esr1}$ **(f)** and cMPOA$^{Esr1}$ **(g)** cells aligned to the onset of male investigation or female investigation.

**(h)** Mean GCaMP6f signals during male investigation and female investigation.

**(i-j)** Average PETHs of GCaMP6f signals of rMPOA$^{Esr1}$ **(i)** and cMPOA$^{Esr1}$ **(j)** cells aligned to the onset of attacking male or mounting female.

**(k)** Mean GCaMP6f signals during attack and mount.

All data are presented as mean ± s.e.m. **(c-k)** n=6 (rMPOA) and 5 (cMPOA) mice. **(e, h and k)** Two-way RM ANOVA with Sidak's multiple comparisons test; *$p$<0.05; **$p$<0.01; ***$p$<0.001; Otherwise, p>0.05.

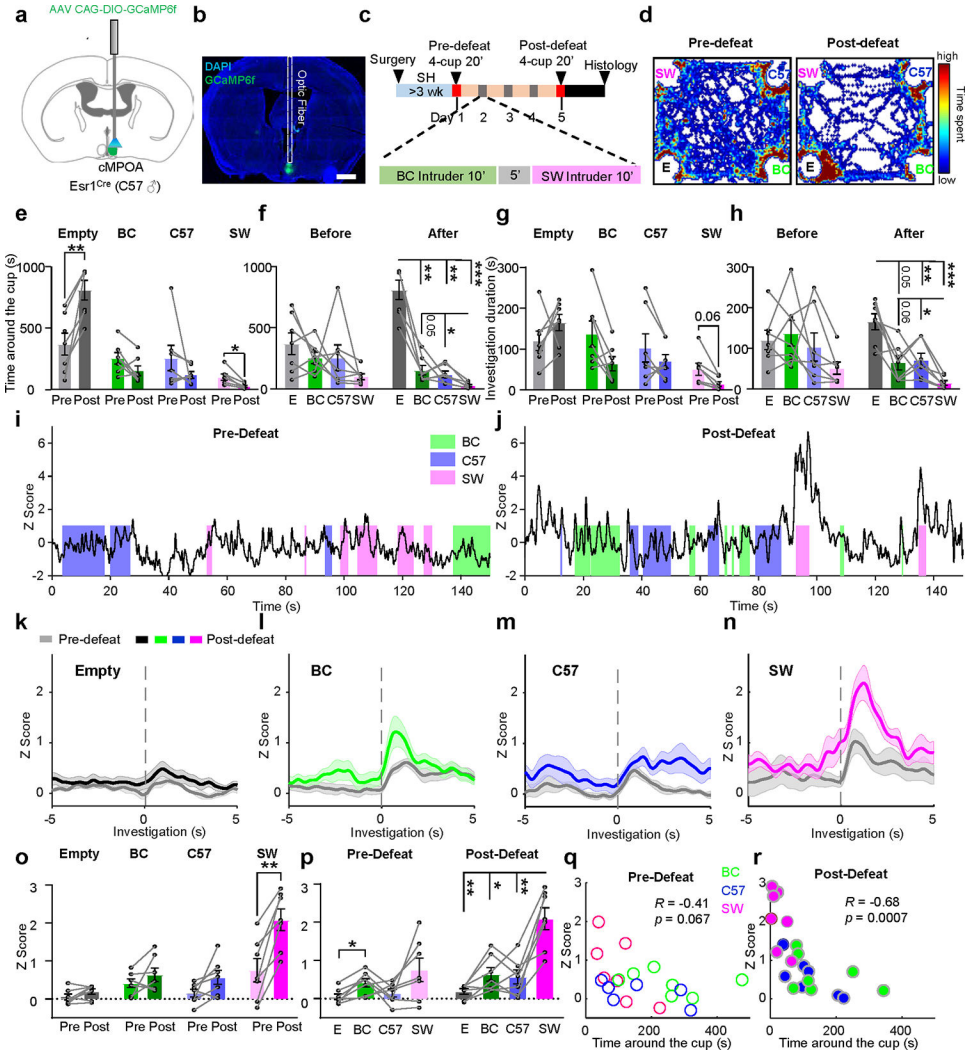


**Figure 2: Male cMPOA$^{Esr1}$ cells encode perceived RHP of a male opponent.**

**(a)** Viral strategy for GCaM6f expression in cMPOA$^{Esr1}$ cells.

**(b)** Representative histology images showing the expression of GCaMP6f in cMPOA$^{Esr1}$ cells. Scale bar: 1 mm.

**(c)** Experimental timeline.

**(d)** Representative heatmaps showing body center location of a test mouse during the 4-cup test before and after defeat.

**(e-f)** The time spent around different cups during the 4-cup test before and after defeat.

**(g-h)** Investigation duration towards different cups during the 4-cup test before and after defeat.

**(i-j)** Representative GCaMP6f recording traces (Z scored ΔF/F) of cMPOA$^{Esr1}$ cells during investigation of different cups before **(i)** and after defeat **(j)**. Color shades indicate investigation events. Empty cup investigation events were not marked.

**(k-n)** Average PETHs of GCaMP6f signals of cMPOA$^{Esr1}$ cells aligned to the onset of investigation of empty cup **(k),** BC cup **(l),** C57 cup **(m)** and SW cup **(n)** before and after defeat.

**(o-p)** Mean GCaMP6f responses during investigation of different cups before and after defeat.

**(q-r)** Scatter plots showing the relationship between mean GCaMP6 activity during cup investigation and total time around spent around the cup during the 4-cup test before **(q)** and after defeat **(r)**.

All data are presented as mean ± s.e.m. n=7 mice. Two-way RM ANOVA with Sidak's multiple comparisons test (**e, g, and o**), Two-way RM ANOVA with Tukey's multiple comparisons test (**f, h, and p**) and Pearson's cross correlation (**q and r**); *$p$<0.05; **$p$<0.01; ***$p$<0.001; Otherwise, p>0.05.

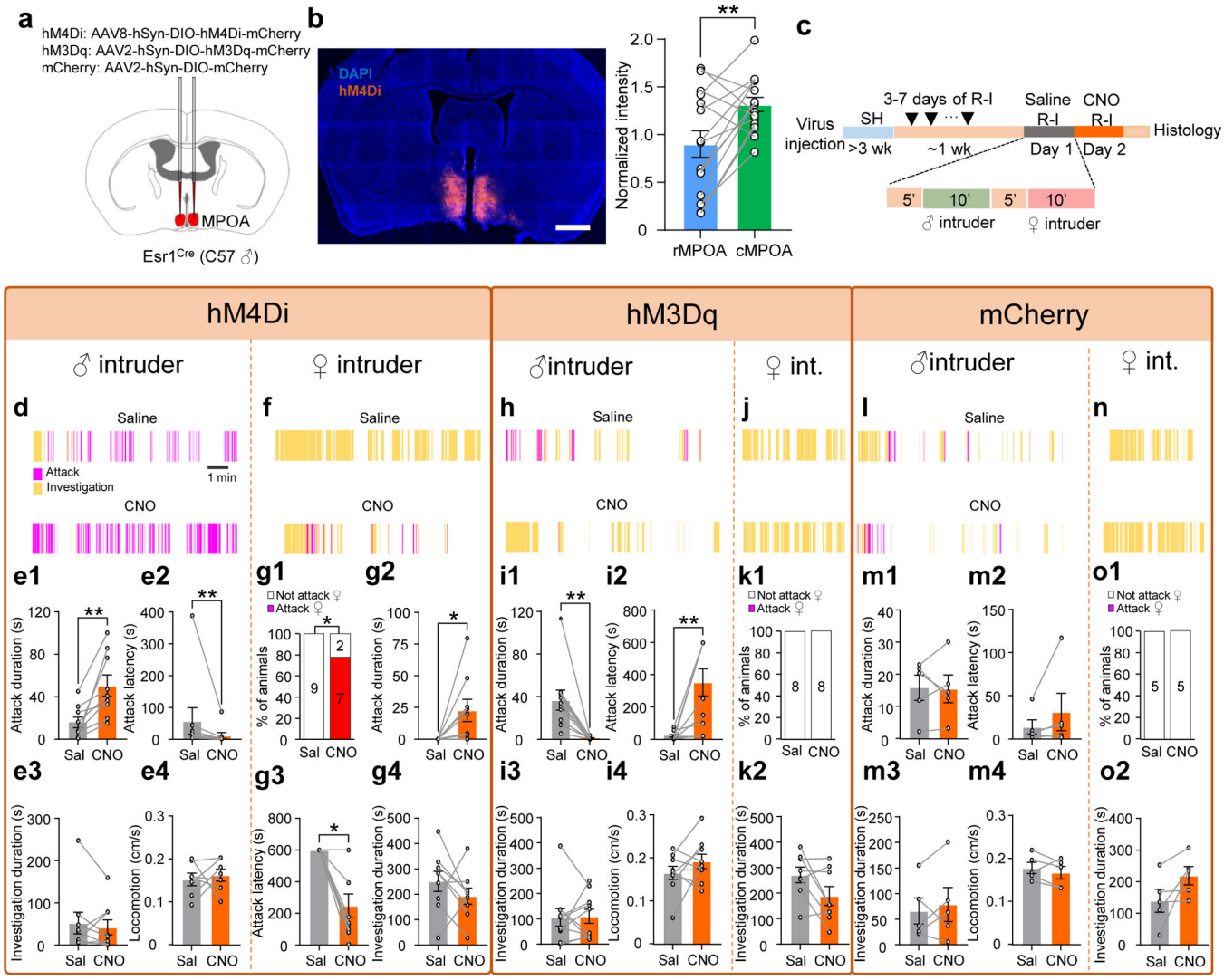


**Figure 3. cMPOA$^{Esr1}$ cells bi-directionally modulate male aggression**

**(a)** Viral strategy for chemogenetic manipulation of cMPOA$^{Esr1}$ cells.

**(b)** A representative image showing the expression of hM4Di-mChery in cMPOA$^{Esr1}$ cells and the quantification of average fluoresce intensity in the rMPOA and cMPOA of hM4Di and hM3Dq animals. Scale bar: 1 mm.

**(c)** Experimental timeline.

**(d)** Representative raster plots showing attack and investigation towards a male intruder after i.p. injection of saline (top) or CNO (bottom) of a hM4Di test male mouse.

**(e)** Attack duration **(e1),** latency to attack **(e2)** and investigation duration **(e3)** towards a male intruder after saline or CNO injection into hM4Di male mice. **(e4)** Locomotion velocity (cm/s) on hM4Di test male mice after saline or CNO injection.

**(f)** Representative raster plots showing behaviors towards a female intruder after i.p. injection of saline (top) or CNO (bottom) of a hM4Di test male mouse.

**(g1)** The percentage of hM4Di test mice that attacked a female intruder after i.p. injection of saline or CNO.

**(g2-g4)** Attack duration **(g2),** latency to attack **(g3)** and investigation duration **(g4)** towards a female intruder after saline or CNO injection into hM4Di male mice.

**(h-i)** Results from hM3Dq test male animals towards male intruders. Follow conventions in **d-e.**

**(j)** Representative raster plots showing behaviors towards a female intruder after i.p. injection of saline (top) or CNO (bottom) of a hM3Dq test male mouse.

**(k1)** The percentage of hM3Dq test mice that attacked a female intruder after i.p. injection of saline or CNO.

**(k2)** Investigation duration towards a female intruder after saline or CNO injection into hM3Dq male mice.

**(l-o)** Results from mCherry animals. Follow conventions in **h-k**.

All data are presented as mean ± s.e.m. **(b)** n=15 mice; **(e1, e2, e3, g, i4)** n=9 mice; **(e4)** n=7 mice; **(i1, i2, i3)** n = 10 mice; **(k)** n = 8 mice; **(m, o)** n = 5 mice. Two-tailed paired *t*-test **(b, e1, e4, g4, i4, k2, m1, m3, m4 and o2)**, two-tailed Wilcoxon matched-pairs signed rank test **(e2, e3, g2, g3, i1, i2, i3 and m2)**, and two-sided McNemar's test **(g1, k1 and o1)**; *$p$<0.05; **$p$<0.01; Otherwise, p>0.05.

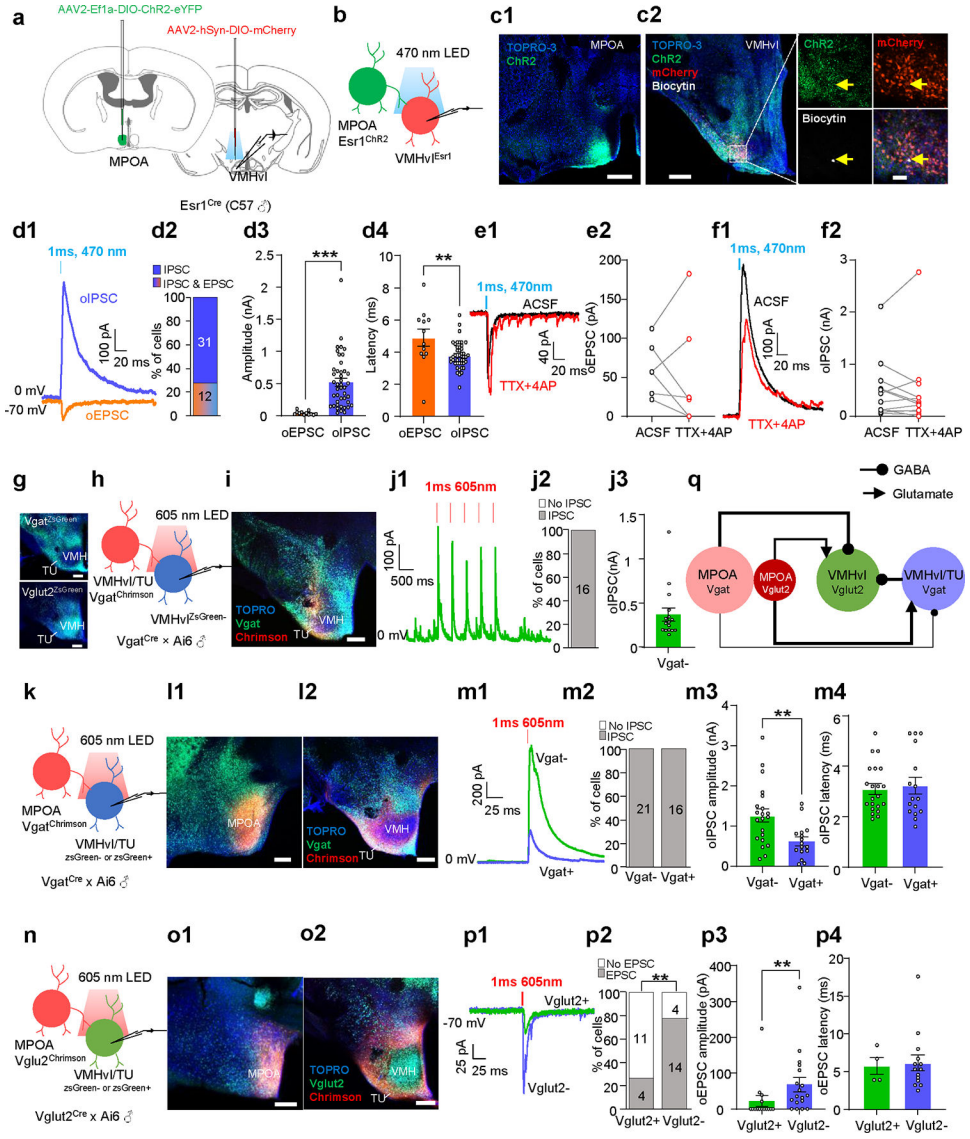


**Figure 4: MPOA cells primarily provide inhibitory inputs to VMHvl cells.**

**(a-b)** ChR2-assisted circuit mapping.

**(c)** ChR2-EYFP expression in cMPOA$^{Esr1}$ cells (**c1**) and their terminals (**c2, left**). A biocytin-filled VMHvl cell **(c2, right)**.

**(d1)** Example light-evoked EPSC (oEPSC) and IPSC (oIPSC).

**(d2)** The percentage of VMHvl$^{Esr1}$ cells showing oIPSC only or both oIPSC and oEPSC.

**(d3-d4)** The amplitude **(d3)** and latency **(d4)** of oEPSCs and oIPSCs in VMHvl$^{Esr1}$ cells.

**(e-f)** No change in oEPSC **(e2)** or oIPSC **(f2)** amplitude of VMHvl$^{Esr1}$ cells before and after TTX+4-AP. **e1 and f1** show sample traces.

**(g)** Histology images from Vgat$^{Cre}$×Ai6 (**top**) and Vglut2$^{Cre}$×Ai6 (**bottom**) mice at VMHvl/TU level.

**(h)** Strategy to investigate TU-VMHvl projection.

**(i)** Chrimson-tdTomato expression in TU Vgat cells in a Vgat$^{Cre}$×Ai6 mouse.

**(j1)** Example oIPSC.

**(j2)** oIPSC in all recorded Vgat− VMHvl cells.
**(j3)** The amplitude of oIPSCs in recorded Vgat− VMHvl cells.
**(k, n)** Strategies to investigate MPOA–VMHvl/TU GABAergic **(k)** and glutamatergic **(n)** projections.
**(l1, l2, o1, o2)** Chrimson-tdTomato expression in MPOA Vgat+ **(l1)** and Vglut2+ **(o1)** cells, and their terminals in VMHvl/TU **(l2, o2)** in $Vgat^{Cre}$×Ai6 **(l)** and $Vglut2^{Cre}$×Ai6 **(o)** mice.
**(m1, p1)** Example oIPSC **(m1)** and oEPSC **(m2)**.
**(m2)** The percentage of Vgat− VMHvl and Vgat+ TU cells showing oIPSC.
**(m3, m4)** The amplitude **(m3)** and latency **(m4)** of oIPSCs in Vgat− VMHvl and Vgat+ TU cells.
**(p2)** The percentage of Vglut+ VMHvl and Vglut2- TU cells showing oEPSC.
(**p3-p4)** The amplitude **(p3)** and latency **(p4)** of oEPSCs in Vglut2+ VMHvl and Vglut2- TU cells.
**(q)** Summary of the circuit among $MPOA^{Vgat}$, $MPOA^{Vglut2}$, VMHvl and TU cells.
Scale bars: 500 μm (**c1**), 250 μm **(c2 left**, **g, i, l, o)** and 50 μm **(c2**, **right).** Error bars: ± s.e.m. **(d3, d4)** n=12(oEPSC) and 43(oIPSC) cells/5 mice. **(e2)** n=6 cells/3 mice. **(f2)** n=11 cells/4 mice. **(j3)** n=16 cells/4 mice. **(m2-m4)** n=21(Vgat−) and 16(Vgat+) cells/7 mice. **(p3)** n=15(Vglut2+) and 18(Vglut2−) cells/3 mice. **(p4)** n=4(Vglut2+) and 14(Vglut2−)/3 mice. Two-tailed unpaired *t*-test **(d3, d4 and m3)**, two-tailed Wilcoxon matched-pairs signed rank test **(e2, f2)**, two-tailed Fisher's exact test **(m2, p2)**, and two-tailed Mann Whitney test **(m4, p3, p4)**; $^{**}p<0.01$; $^{***}p<0.001$; Otherwise, $p>0.05$.

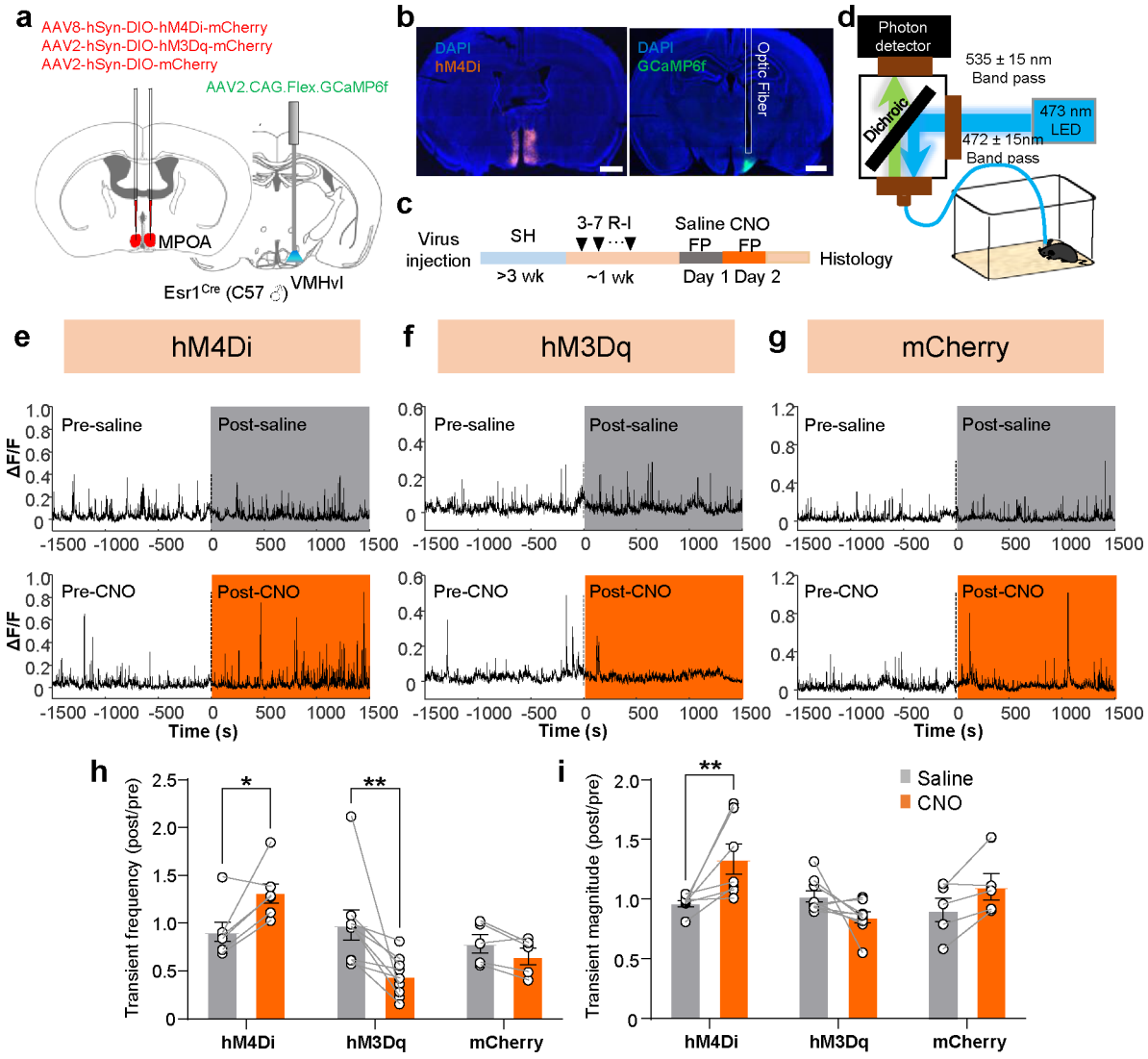


**Figure 5: cMPOA$^{Esr1}$ cells negatively modulate VMHvl$^{Esr1}$ cell activity.**

**(a)** Viral strategy for simultaneous chemogenetic manipulation of cMPOA$^{Esr1}$ cells and recording of GCaMP signal from VMHvl$^{Esr1}$ cells.

**(b)** Representative histology images showing the expression of hM4Di-mchery in cMPOA$^{Esr1}$ cells and GCaMP6f in VMHvl$^{Esr1}$ cells. Scale bars: 1 mm.

**(c)** Experimental timeline.

**(d)** Light path of the fiber photometry setup.

**(e-g)** Representative GCaMP6f recording (ΔF/F) traces from hM4Di **(e)**, hM3Dq **(f)** and mCherry control **(g)** mice before and after i.p. injection of saline (top) and CNO (bottom).

**(h and i)** Normalized GCaMP6f transient frequency **(h)** and magnitude **(i)** of VMHvl$^{Esr1}$ cells in hM4Di, hM3Dq and mCherry control mice.

All data are presented as mean ± s.e.m. n=7 (hM4Di), 9 (hM3Dq) and 5 (mCherry) mice. **(h and i)** Two-way RM ANOVA with Sidak's multiple comparisons test; *$p$<0.05; **$p$<0.01; Otherwise, p>0.05.

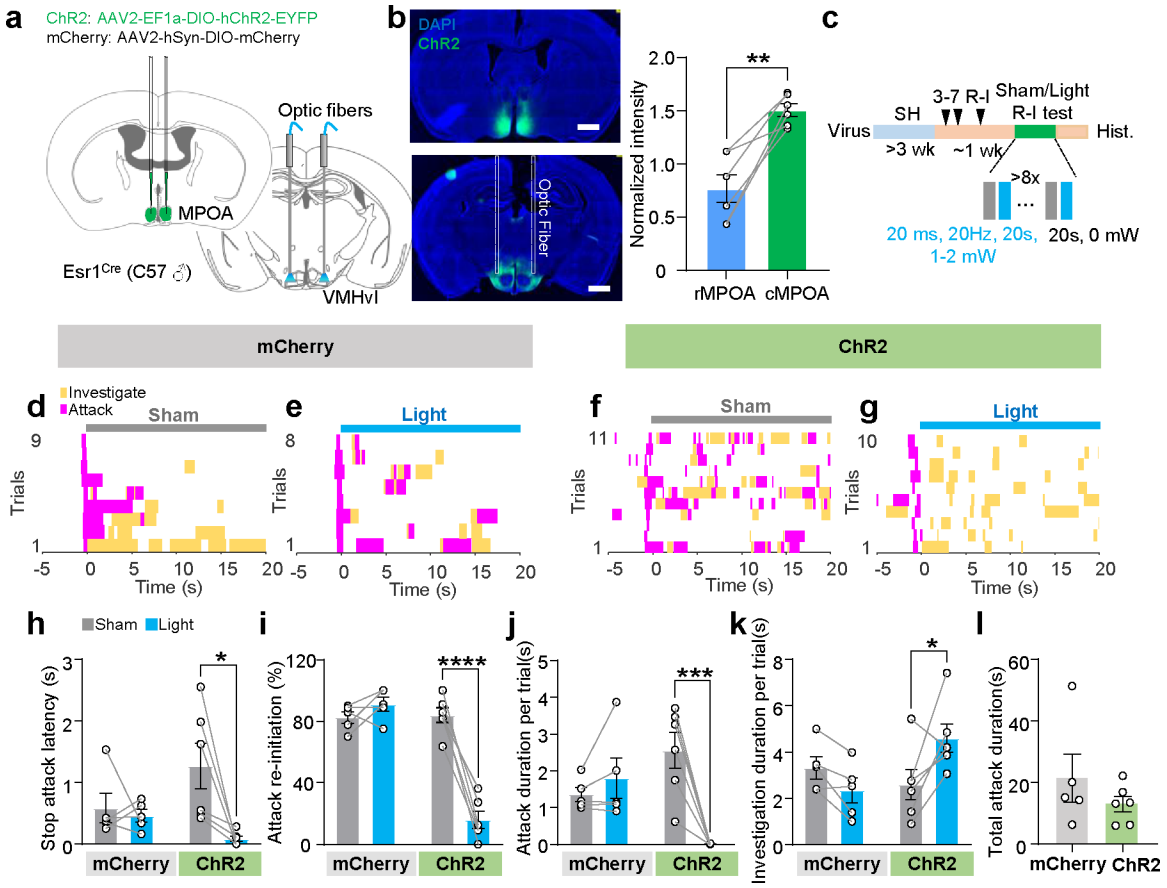


**Figure 6: Optogenetic activation of cMPOA$^{Esr1}$-VMHvl terminals suppresses aggression toward a weak male intruder.**

**(a)** Viral strategy for optogenetic activation of cMPOA$^{Esr1}$-VMHvl terminals.

**(b)** Representative histology images showing the expression of ChR2-eYFP in cMPOA$^{Esr1}$ cells and ChR2-eYFP fibers from MPOA$^{Esr1}$ to VMHvl (left) and the average fluorescence intensity in the rMPOA and cMPOA (right). Scale bars: 1 mm.

**(c)** Experimental timeline.

**(d, e)** Representative raster plots showing attack and investigation towards a male intruder in mCherry control mice aligned to sham **(d)** and light **(e)** onsets.

**(f, g)** Representative raster plots from a ChR2 test mouse.

**(h-k)** The stop attack latency **(h),** attack re-initiation probability **(i),** attack duration per trial **(j),** and investigation duration per trial **(k)** towards male intruders during sham and light stimulation of mCherry control and ChR2 test mice.

**(l)** The accumulated attack duration towards male intruders during R-I tests in mCherry and ChR2 test mice.

All data are presented as mean ± s.e.m. **(b):** n=6 mice; **(h-l):** n=5 (mCherry) and 6 (ChR2) mice. Two-tailed paired *t*-test **(b),** two-way RM ANOVA with Sidak's multiple comparisons test **(h-k)**, and two-tailed unpaired *t*-test **(l)**; **p*<0.05; ****p*<0.001; *****p*<0.0001; Otherwise, p>0.05.

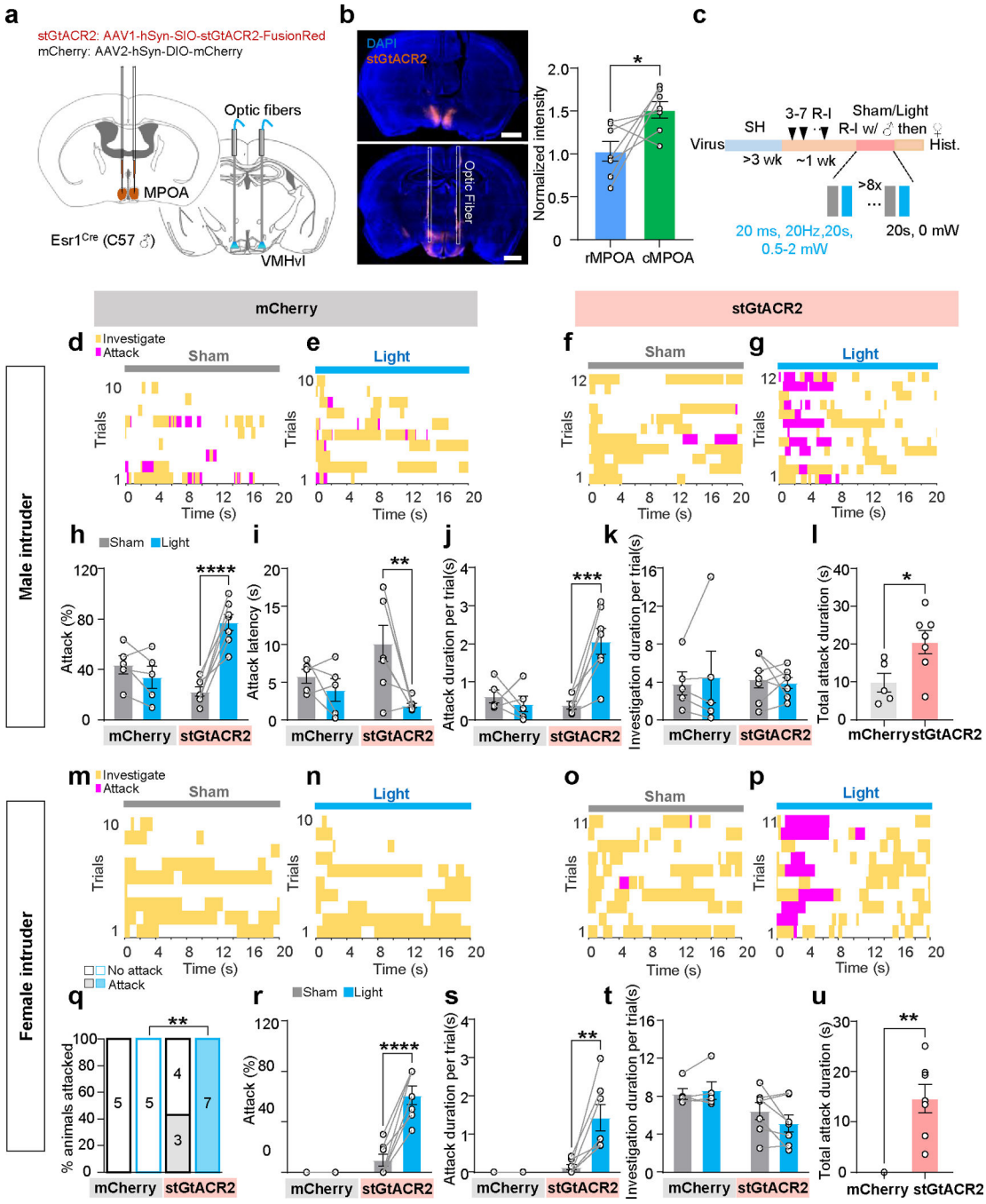


**Figure 7: Optogenetic inactivation of cMPOA$^{Esr1}$-VMHvl projection promotes attack in aggressive male mice.**

**(a)** Viral strategy for optogenetic inactivation of cMPOA$^{Esr1}$-VMHvl terminals.

**(b)** Representative histology images showing the expression of stGtACR2-FusionRed in cMPOA$^{Esr1}$ cells and stGtACR2-FusionRed fibers in VMHvl. Scale bars: 1 mm.

**(c)** Experimental timeline.

**(d-e)** Representative raster plots showing attack and investigation towards a male intruder of a mCherry mouse aligned to sham **(d)** and light **(e)** onsets.

**(f-g)** Representative raster plots of a stGtACR2 mouse.

**(h-k)** The attack probability **(h)**, the latency to attack **(i)**, the average attack duration per trial **(j)** and the average investigation duration per trial **(k)** towards a male intruder during sham or light stimulation in mCherry control and stGtACR2 test mice.

**(l)** The total attack duration towards a male intruder during the R-I test in mCherry and stGtACR2 mice.

**(m-p)** Representative raster plots showing attack and investigation towards a female intruder aligned to sham (**m, o**) and light (**n, p**) onsets of a mCherry (**m, n**) and a stGtACR2 mouse (**o, p**).

**(q)** The percentage of mCherry and stGtACR2 mice that attacked the female intruder during sham and light stimulation trials.

**(r-t)** The attack probability **(r)**, the average attack duration per trial **(s)** and the average investigation duration per trial **(t)** towards a female intruder during sham or light stimulation in mCherry control and stGtACR2 test mice.

**(u)** The total attack duration towards a female intruder of mCherry and stGtACR2 mice.

All data are presented as mean ± s.e.m. **(b):** n=7 mice; **(h-l, q-u):** n=5 (mCherry) and 7 (stGtACR2) mice. Two-tailed paired *t*-test **(b),** two-way RM ANOVA with Sidak's multiple comparisons test **(h, i, j, k, r, s and t)**, two-tailed unpaired *t*-test **(l)**, two-tailed Fisher's exact test **(q)**, and two-tailed Mann Whitney test **(u)**; *$p$<0.05; **$p$<0.01; ***$p$<0.001; ****$p$<0.0001; Otherwise, p>0.05.

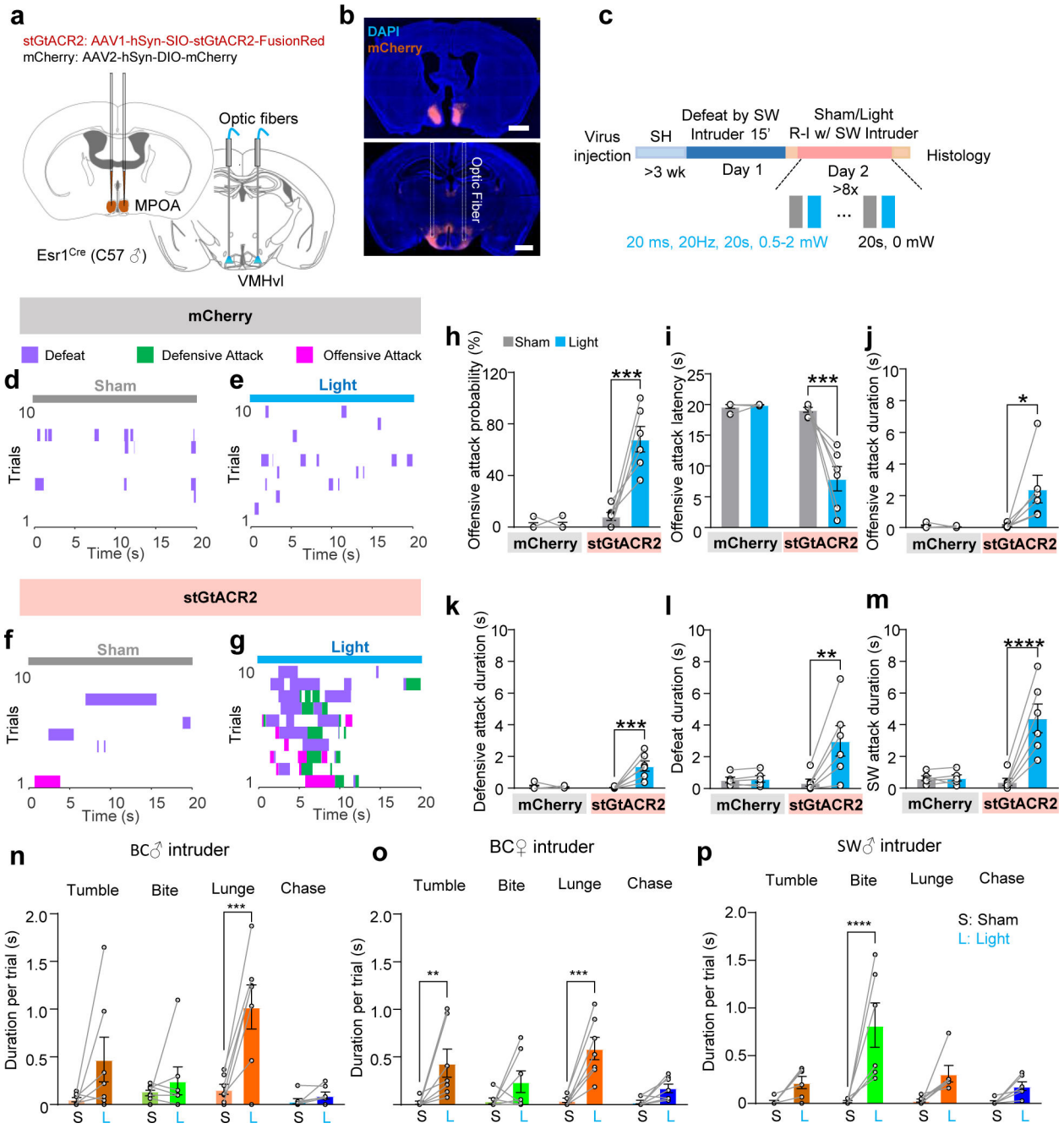


**Figure 8: cMPOA$^{Esr1}$-VMHvl inactivation promotes aggression towards stronger opponents.**

**(a)** Viral strategy for optogenetic inactivation of cMPOA$^{Esr1}$-VMHvl terminals.

**(b)** Representative histology images showing the expression of mCherry in cMPOA$^{Esr1}$ cells and MPOA$^{Esr1}$ terminals in VMHvl. Scale bars: 1 mm.

**(c)** Experimental timeline.

**(d-g)** Representative raster plots showing offensive attack, defensive attack and defeat during encounter with a SW male intruder aligned to sham **(d, f)** and light **(e, g)** onset in mCherry **(d, e)** and stGtACR2 **(f, g)** mice.

**(h-k)** The offensive attack probability **(h)**, the latency to initiate offensive attack **(i)**, the average offensive attack duration per trial **(j),** and the average defensive attack duration per trial **(k)** towards the SW aggressive male intruder during sham and light stimulation of mCherry control and stGtACR2 test mice.

**(l)** The average duration of being defeated by the SW intruder per light/sham trial of mCherry and stGtACR2 mice.

**(m)** The average attack duration of SW intruder per light/sham trial against mCherry and stGtACR2 mice.

**(n-p)** The average duration of various actions related to attack during each 20-s sham and light trials when the test animals encounter BC male (n), BC female (o) and SW male (p) intruders.

All data are presented as mean ± s.e.m. **(h-m)** n=5 (mCherry) and 6 (stGtACR2) mice. **(n, o)** n=7 mice; **(p)** n = 6 mice. **(h-p)** Two-way RM ANOVA with Sidak's multiple comparisons test. *$p$<0.05; **$p$<0.01; ***$p$<0.001, ****p<0.0001; Otherwise, p>0.05.